THE EFFECT OF MICROSTRUCTURE ON THE FRETTING FATIGUE BEHAVIOR OF NICKEL ALLOY IN-100

THESIS

Erik C. Saladin, Captain, USAF

AFIT/GMS/ENY/07-M02

DEPARTMENT OF THE AIR FORCE
AIR UNIVERSITY

AIR FORCE INSTITUTE OF TECHNOLOGY

Wright-Patterson Air Force Base, Ohio

The views expressed in this thesis are those of the author and do not reflect the official policy or position of the United States Air Force, Department of Defense, or the United States Government.

AFIT/GMS/ENY/07-M02

The Effect of Microstructure on Fretting Fatigue Behavior of Nickel Alloy IN-100

Thesis

Presented to the Faculty

Department of Aeronautics and Astronautics

Graduate School of Engineering and Management

Air Force Institute of Technology

Air University

Air Education and Training Command

In Partial Fulfillment of the Requirements for the

Degree of Master of Science in Aerospace Engineering

Erik Saladin at AFIT, BSME

Captain, USAF

March 2007

AFIT/GMS/ENY/07-M02

The Effect of Microstructure on Fretting Fatigue Behavior of Nickel Alloy IN-100

Erik Saladin at AFIT, BSME

Captain, USAF

Approved: Date:

_____ _____
Shankar Mall (Chairman)

_____ _____
Michael Heil (Member)

_____ _____
Vinod Jain (Member)

AFIT/GMS/ENY/07-M02

Abstract

This thesis studied the effect of microstructure on the fretting fatigue behavior of IN-100. First, fretting and plain fatigue S-N curves were determined over a large range of applied stress at an identical R-ratio and for fretting tests, with a constant contact load. It was found that fretting fatigue reduces the cycles to failure compared to plain fatigue. The half contact width was found for the specimens, the crack initiation angle was found to be 40° and the crack initiation location was at the trailing edge of contact for the fretting specimens. Computational work included finding the stress profile in the contact region using an analytical method and finite element method. The analytical method computed half contact width and was found to be in good agreement with experimental half contact width. The stress profiles produced from each method were compared and found to be in good agreement. The stress state was used to find the Modified Shear Stress Range (MSSR) Parameter. The MSSR parameter produced results in good agreement with the experimental data for crack initiation location and fatigue life. This study found microstructure did not have an effect on the MSSR parameter for IN-100. This study also found MSSR data developed for titanium alloys did not adequately represent IN-100. The parameter also gave reasonable agreement with the experimental finding for crack initiation angle. A microstructural evaluation was done between the 7 micron grain sized material of this study and an oblong, 10 by 50 micron grained microstructure IN-100 from a previous study. The study found microstructure did have an effect on crack initiation and crack propagation, with the coarser grain structure performing better in fretting fatigue. The coarser grain structure allowed a longer initiation and crack propagation time. Impeded crack development by a more tortuous crack path is a possible reason. These findings were different than in titanium alloys, where a finer grain structure allowed a longer crack initiation time by impeding crack development with a more tortuous crack path.

Acknowledgements

I would like to thank my advisor, Dr. Mall for the opportunity to work under his supervision, I have learned much from him and the papers he has written. I would like to thank my wife, parents and brother for believing in me and supporting my effort to get a master's degree. I would like to thank John Porter, Dr. Salbelkin, Mohammed Almajali and Kasey Scheel for working with me and teaching me the ropes. Finally, I would like to thank the Air Force for the opportunity to attend the awesome program at AFIT.

Erik Saladin, Capt, USAF

Table of Contents

List of Figures

List of Tables

List of Symbols

a	Half contact width
b	Specimen half thickness
c	Stick zone boundary
d	Tensile bar thickness
E	Modulus of elasticity
f	Coefficient of friction
K_1	First Ruiz parameter
K_2	Second Ruiz parameter
ΔK_{Ic}	Critical stress intensity range
N	Number of cycles
N_f	Number of cycles to failure
P	Normal load
p_o	Maximum pressure in the contact zone
Q	Shear load
Q_{max}	Maximum shear load
Q_{min}	Minimum shear load
r	Radius of curvature
R	Stress ratio
σ	Stress

δ	Slip at interface
γ'	Nickel-aluminum precipitate
σ_{axial}	Axial stress applied to tensile bar
$\sigma_{\max}$	Maximum applied axial stress
$\sigma_{\min}$	Minimum applied axial stress
σ_{xx}	Axial stress in the contact zone
σ_{yy}	Transverse stress in the contact zone
$\Delta\sigma$	Stress range
τ	Surface shear stress
$\tau_{\max}$	Maximum shear
$\tau_{\min}$	Minimum shear
τ_{xy}	Shear stress in contact zone
$\Delta\tau$	Shear stress range
$\Delta\tau_{crit}$	Shear range in the critical range
υ	Possion's ratio

I. Introduction

This chapter will give a short introduction to this study. A short explanation of fretting fatigue will be given followed by a discussion of fretting fatigue on nickel alloys and some of the factors affecting fretting. The objectives of this study will be given and finally the methods used in this study will be introduced.

1.1 Fretting Fatigue

Fretting can occur when two structural elements are in contact and have a normal load and a cyclic stress applied to them concurrently. This contact leaves two stressed surfaces in a state of micro slip relative to each other. This slip is often caused by a small amplitude oscillatory motion and results in reduction in the fatigue life of the materials involved. The combined loading on the structural elements induces tensile and shear stresses by the fretting action. Often in metals, the oxide layer on the metals is disrupted and unprotected metal to metal contact results. Local welds can form, causing metal to be removed from the original surface. This adhesive damage leads to the formation of a crack, often at the edge of the contact region. The crack often advances into the material at an angle; and is described as a Stage I short crack, advancing by a combination of the normal load and cyclic stress. Soon the crack turns and following Paris law, grows in a plane perpendicular to the cyclic stress; this Stage II crack grows due only to the applied cyclic load. Finally, the crack leads to a failure when the ΔK_{1C} of the material is reached.

Fretting fatigue is found in riveted and bolted joints, dove tail joints in machinery and others see Figure 1.1. The loads applied to the structural elements are often from high vibrational frequencies and a high mean stress from a source such as clamping force in a bolted joint. Frequently bolted, riveted and dovetail joints are difficult to completely inspect. Many surfaces in the joints are covered leaving joint disassembly as the only option for full inspection.

1.2 Nickel Alloys and Fretting

Fretting has been studied in a variety of different materials. These include titanium alloys, aluminum alloys, carbon steels and others. However, the work on nickel-based alloys is less advanced than some of the other materials mentioned here. As nickel-based alloys have been specified more and more for high temperature jet turbine engine applications it is becoming more relevant to understand the failure mechanics of these materials. Nickel based alloys have many advantages for use in high temperature applications [1] such as a low thermal expansion and a nearly constant modulus of elasticity in a limited temperature range. Also, nickel alloys such as IN-100 have very good creep characteristics, fracture, thermo-elastic properties and are castable. Since casting is ideal to produce the complex shapes needed for effective aerodynamics and for other properties mentioned, nickel alloys are considered ideal for high temperature applications. Unfortunately, Linear Elastic Fracture Mechanics is insufficient to describe the failure of nickel alloys and cannot be relied upon for predicting service life. For this reason a better understanding of fretting fatigue is being pursued. This study, using IN-

100, a fine grained nickel alloy, is intended to contribute to the much larger effort of understanding fretting fatigue and more specifically to build a basic understanding of IN-100 fretting fatigue at room temperature. IN-100 is used in turbine disks as a polycrystalline material and turbine blades in gas turbine engines as a monocrystalline material [2], see Figure 1.2.

1.3 Factors Affecting Fretting

Fretting action is defined as a cyclic sliding contact from $5\,\mu m$ to $50\,\mu m$. The contact has a sliding motion at the edges and stick in the middle, creating a partial slip condition [3]. Many factors contribute to fretting fatigue. The most important ones are contact pressure, magnitude of slip, peak pressure between components, contact semi-width and cyclic stress amplitude. During fretting action local areas of high stress are created. Some of the factors causing the high stress are measurable. For this study normal load, bulk stress from the applied cyclic load, shear tangential stress, relative slip, coefficient of friction and contact geometry will be derived or measured directly. In fretting, cracking begins very early, but the cracks close and propagate very little during the beginning. Initially, contact pressure at the contact edge is very high, but as fretting wears the edge away, the stress reduces and cracks gradually start to propagate. The action of small cracks initiated at the contact edge defines fretting. If the cracks cease to propagate, then the fretting action is considered below the fretting fatigue threshold. If the cracks propagate and eventually lead to failure, then the fretting action is considered

above the fretting fatigue threshold. It has been shown that microstructure can affect the fretting fatigue properties in metals such as titanium alloys.

1.4 Objectives of Study

Currently there are many unknown factors that affect material service life. Fretting is one of the factors among others. This study will investigate the affect of fretting fatigue versus plain fatigue, recording the differences and the magnitude of the effect. This study is intended to baseline the fatigue and fretting fatigue properties of IN-100 at room temperature for later advanced studies that include elevated temperatures and other advanced factors. The intent is to define the S-N curve for fretting fatigue and also plain fatigue. The effect if any, of microstructure on fretting fatigue is also not well understood. This study would also like to contribute to understanding the effect of microstructure on the fretting fatigue properties of nickel alloys by recording the microstructure of the material tested and compare the results versus another microstructure of IN-100. Further, this study would like to compare the microstructural effects in IN-100 to known microstructural effects in fretting fatigue of titanium alloys.

1.5 Methods of Study

Since fretting fatigue happens in a variety of components and in a variety of geometries a simplified model is used for research. Several models are currently used to research fretting. The model used in this study is the cylinder-on-flat model. This model

is less severe than the flat-on-flat model and the results of the two should not be considered the same. Two loads are applied to the flat sample, a tensile bar loaded into a uni-axial servo-hydraulic machine. A cyclic axial load is applied to the tensile bar by the servo-hydraulic machine, and a normal load is applied to the tensile sample through the cylindrical fretting pad. The tensile bar is gripped at the top and held stationary at this grip, the cyclic loading is applied at the bottom grip. The fretting load is applied by a spring loaded tension mechanism and is applied to the tensile bar by a set of cylindrical ended fretting pads. The normal load (P) causes a shear (Q) on the sample, Q can be measured by taking the difference of the measured load at the top grip and the measured load at the bottom grip, and dividing by two. Q is useful among other variables in determining the stresses acting in the fretting contact area.

Figure 1.1 A dovetail joint

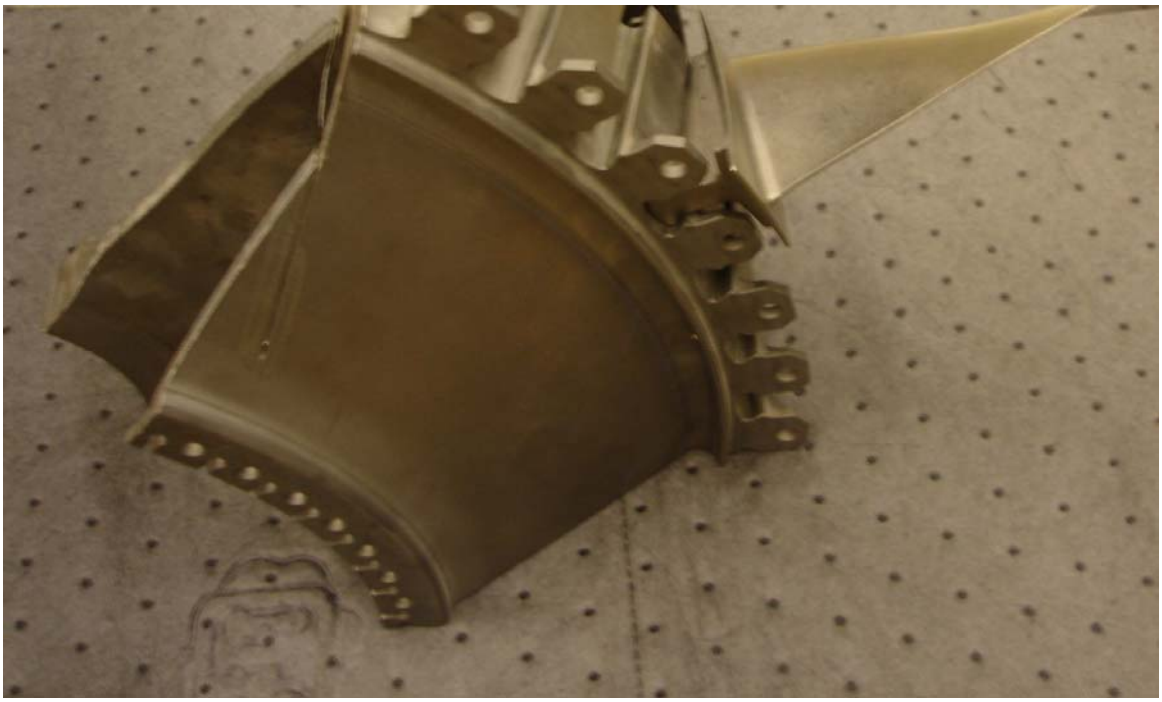

Figure 1.2 Fan blade and disk

II. Background

It is the belief of this author that currently very little work in fretting has been done specifically in nickel alloys. So this background will discuss the contact mechanics of fretting as it has been applied to other materials as a starting point for analysis of IN-100. In addition, a discussion of crack nucleation and growth will be provided. Very little is known about crack nucleation in fretting so only ideas will be outlined. Next, the analysis techniques used in this study will be discussed. Then the microstructure of the material will be discussed and following that a discussion of fretting parameters. Finally, for completeness, a short overview of studies done specifically with nickel-based alloys will be reviewed.

2.1 Contact Mechanics

This section will describe the test sample, fretting pads and general test set-up in detail. The test sample is a 127 mm long tensile bar, the center section of the bar is 54.6 mm long. The average thickness, d, of the bar is 3.66 mm, the half thickness is indicated by the letter b. The finish on the bar was finely ground to produce a smooth finish and the corners of the bar have been ground to round them slightly and finish them without a burr. The fretting pads are 9.525 mm square and have a 50.8 mm radius, r, with a ground finish. The tensile bar is loaded into the uni-axial servo hydraulic machine and a cyclic load is applied to the tensile bar, the load produces the stress, σ_{axial}, in the tensile bar. The fretting pads are pressed against the sample with a normal load P. The applied cyclic

load stretches and relaxes the tensile bar and the normal load P arrests part of the stretching in the upper part of the tensile bar, this difference in applied load is called Q. The result of this cyclic stretch and release is a small movement under the fretting pads, leaving a small scar with a zip fastener like appearance. The half-thickness of the scar is indicated by the letter a, see figure 2.1.

2.2 Crack Nucleation and Growth

To begin to discuss the fretting action in more detail, first it is best to remind the reader that crack nucleation in fretting is not well understood. There are ideas about the relationships between the fretting scar and contact mechanics but no single definitive theory. This paper will briefly describe one of those ideas and then move onto the better understood growth phase of the crack. One model used to describe the nucleation of cracks is the Persistent Slip Band Model proposed by Venkataraman et al. [4] and Mura et al [5]. The basic idea of the model is to imagine slip happening along slip bands, usually a slip region is normally adhered and only slipping part of the time, once the slip has occurred, the band returns to the state of adhesion. In the Persistent Slip Band Model, a slip plane will occur during one stretching of the tensile bar, when the bar is allowed to relax the slip plane will return to a state of adhesion and a new slip plane will form next to the old slip plane. This motion continues with new slip planes forming with each stretching and relaxing of the tensile sample. These slip planes cause material to be scraped into small extrusions at the edges of the slip planes. As the extrusions form, the slip plane itself leaves an intrusion into the metal. As the fretting action continues these

intrusions and extrusions smear away and reform constantly. As this motion happens, a small amount of strain energy is stored and a small amount of heat is released. With time, it becomes energetically favorable for a crack to form, the crack will continue to grow until it reaches a size equaling about 1-3 grain sizes. Three main variables determine the cycles to crack initiation, the amplitude of slip, the contact width of the fretting pad, and the length of the slip bands. At this point, it is possible to describe the growth of the crack using fracture mechanics. The above described approach uses a micro-mechanics model to describe the crack initiation phase. Other approaches have been presented using an empirical model to describe the behavior of the bulk material. The objective is to estimate when a crack will grow to the appropriate size to use fracture mechanics.

Once the crack has developed to the size to use fracture mechanics, several ideas have been presented using a crack tip stress intensity factor to describe the crack growth and ultimate failure. For example Sakata [6] used a boundary element method program designed for fretting contact and compared the results of the program to a stress intensity factor based approach to crack development and found good agreement. Hattori [7] used another approach applying a stress intensity factor to crack tips found in the contact area of fretting conditions. This approach suggests fretting fatigue life could be calculated from the crack tip propagation.

For this study an analysis of contact mechanics by Hills and Nowell [8] is applied for a cylinder on flat configuration. The solution is based on the assumption of infinite

boundaries leaving the fretting area. In the following analysis, σ_{axial} is used to represent the axial stress, P is used for the applied normal load, Q is used for the tangential load, A is the cross-sectional area of the specimen, b is the specimens half thickness, and r is the radius of the fretting pad. The following equation governs the contact region:

$$\frac{1}{A^*}\frac{\delta h(x)}{\delta x} = \frac{1}{\pi}\int \frac{p(\varsigma)}{x-\varsigma} d\varsigma - \beta q(x) \qquad (2.1)$$

In the above equation, h(x) =v1(x)-v2(x) and defines the amount the overlap of the two bodies if they could penetrate each other freely. P is the pressure in the contact zone and q is the surface shear stress. A^* and β are defined by material properties and are:

$$A^* = 2\left(\frac{1-\upsilon_1^2}{E_1} + \frac{1-\upsilon_2^2}{E_2}\right) \qquad (2.2)$$

$$\beta = \frac{1}{2A^*}\left(\frac{1-2\upsilon_1}{E_1} - \frac{1-2\upsilon_2}{E_2}\right) \qquad (2.3)$$

In equations 2.2 and 2.3, E is the Modulus of Elasticity and υ is Poisson's Ratio for each of the contact bodies. If it is assumed that tangential displacement can be defined as:

$$g(x) = u_1(x) - u_2(x) \qquad (2.4)$$

Then, the following equation can be used to govern tangential displacement:

$$\frac{1}{A^*}\frac{\delta g(x)}{\delta x} = \frac{1}{\pi}\int \frac{q(\varsigma)}{x-\varsigma} d\varsigma - \beta p(x) \qquad (2.5)$$

For this study, the tensile sample and fretting pad are made of constituently the same material with a different microstructure. Fortunately, the two materials have similar enough material properties to consider them equal. This leads to some simplifications, it can be seen that equation (2.3) will have a value of 0 if the modulus of elasticity of the two contacting bodies is equal. Also, the displacement of each body will be the same in the stick zone. P(x,y) represents the pressure distribution from the contact load, and is mathematically represented as:

$$p(x) = p_o \sqrt{1 - \left(\frac{x}{a}\right)^2} \qquad (2.6)$$

It can be seen that a pressure distribution made from equation (2.6) will be of a Hertzian form, with x=a and x=–a representing the extremes and x=0 representing the centerline. With p_o representing the peak pressure and defined by either:

$$p_o = \frac{2P}{\pi a} \qquad (2.7)$$

$$p_o = \sqrt{\frac{PE}{2\pi(1-\upsilon^2)R}} \qquad (2.8)$$

In (2.8), R is defined as:

$$R = \frac{\sigma_{\min}}{\sigma_{\max}} \tag{2.8a}$$

To calculate the contact half width a, see figure 2.2, the following equation is used:

$$a = \sqrt{\frac{2P(A^*)}{\pi k}} \tag{2.9}$$

With k defined in terms of the radius of the fretting pad (R_1) and tensile bar (R_2):

$$k = \frac{1}{R_1} + \frac{1}{R_2} \tag{2.10}$$

The axial stress, σ_{xx}, can be defined in terms of x, a and the pressure, p_o:

$$\sigma_{xx} = -p_o \left(\frac{\sqrt{a^2 - x^2}}{a} \right) \tag{2.11}$$

The shear stress distribution along the contact surface can be expressed in terms of a, x, and Q:

$$q(x) = \frac{Q}{\pi\sqrt{a^2 - x^2}} \tag{2.12}$$

Q, the total shear stress along the contact length, can be defined in terms of a, c (see figure 2.3), and p_o by integrating the shear stress distribution as:

$$Q = \frac{fp_o\pi}{2a}\left(a^2 - c^2\right) \tag{2.13}$$

Finally, the stick zone size shown as the fraction, (c/a), can be calculated in terms of Q and P:

$$\frac{c}{a} = \sqrt{\left(1 - \left|\frac{Q}{fP}\right|\right)} \tag{2.14}$$

2.3 Analytical Model

The analytical analysis for this study was performed with a program called Ruiz written by Chan and Lee [9]. Ruiz provided a numerical solution for the Hertizian Peak (eqn 2.7), the contact half width, a, (eqn 2.9) and the axial stress, (eqn 2.11). The solutions generated by Ruiz are valid for fretted test samples with the following condition: b/a<10. In this study, this criterion is violated so Ruiz is only used as an approximation to check the answers generated by other data evaluation methods, in particular, the finite element analysis (FEA) used as a primary solution. The output of Ruiz allows an estimation of the stress state at every location along the contact length. This can be used to compare to the stress state generated by the FEA program. Ruiz uses two parameters to determine the crack nucleation site and propagation, K_1 and K_2 defined as:

$$K_1 = \left(\sigma_T\right)_{\max} (\tau\delta)_{\max} \qquad (2.15)$$

$$K_2 = \left(\sigma_T \tau\delta\right)_{\max} \qquad (2.16)$$

K_2 combines the effect of the surface tangential stress σ_T, shear stress τ and the relative slip at the interface δ, to produce a parameter that predicts how the crack opens and propagates. K_1 uses the max surface tangential stress and the maximum value of shear stress and interface slip to produce a parameter that predicts the frictional work that

nucleates the crack. Combined, the two parameters produce one criterion to describe the crack's initiation and growth.

2.4 Gross Slip and Partial Slip

In fretting, slip and stick zones form, however these two zones don't form at the same time and the slip zone can develop as gross or partial slip. Initially the fretting action begins with the formation of a free slip zone with gross movement between the tensile bar and the pad. In the slip zone, two types of slip can form as the fretting progresses, gross slip or partial slip. In gross slip there is full sliding between the two parts and is called fretting wear. If a state of partial slip forms, there is not gross sliding between the parts but instead small slip zones at the edges of the tensile specimen and the fretting pads with a stick zone formed at the center. This is an ideal and it is possible to have a combination of gross and partial slip.

2.5 Predictive Fretting Fatigue Parameters

Predictive parameters have shown to be advantageous to engineers for plain fatigue specimens and for this reason; it is desirable to develop predictive parameters for fretting fatigue. Parameters can help designers design with better resistance to fretting fatigue and also predict when a failure will occur in a current component, improving safety. The ideal fretting fatigue parameter would predict the crack location, crack initiation angle and fatigue life.

At this time, extending fretting fatigue predictive parameters to nickel-based super alloys is in its infancy. However, there has been work done on determining the suitability of predictive parameters for Ti-6Al-4V and this study will evaluate if one parameter, shown to be the most promising, is suitable to extend to nickel based super alloys.

2.5.1 Critical Plane

In fretting fatigue, crack initiation and nucleation takes place in a multi-axial state of stress in the contact region. Predictive parameters assume that the crack initiation will happen in a particular plane at some angle $\pm 90°$ from the contact line between specimen and fretting pad, referred to as the critical plane. In this critical plane it is assumed that normal stress opens the crack and thus reduces friction between crack surfaces. The shear stress acting at the critical plane induces dislocation movement along slip lines resulting in crack nucleation and growth.

The approach used by predictive parameters is to find the maximum shear strain amplitude and the plane that it acts. Maximum normal stress acting on this plane is also used to determine the effect of the mean stress. The shear stress and normal stress can be determined for any plane if the state of stress $\sigma_{xx}, \sigma_{yy}, \tau_{xy}$ is known for that point. Shear stress can be found from:

$$\tau = -\frac{\sigma_{xx} + \sigma_{yy}}{2}\sin(2\theta) + \tau_{xy}\cos(2\theta) \qquad (2.17)$$

and the normal stress can be found from:

$$\sigma = \frac{\sigma_{xx} + \sigma_{yy}}{2} + \frac{\sigma_{xx} - \sigma_{yy}}{2}\cos(2\theta) + \tau_{xy}\cos(2\theta) \qquad (2.18)$$

In the above two equations, θ is evaluated from -90° to +90°. In general, it is difficult to find $\sigma_{xx}, \sigma_{yy}, \tau_{xy}$ in a fretting fatigue zone. Because of this difficulty, the best way to obtain the state of stress is to use an analytical or finite element method to determine the state of stress in the contact region.

Namjoshi et al [10] argued that the initiation of a fretting crack is the function of shear stress in that plane. The fretting fatigue life is influenced by the normal stress acting on the same plane. Using Ti 6Al 4V, Namjoshi showed that predictive parameters work to show the crack orientation and to a lesser degree of accuracy the crack size.

Madhi [11] used the same alloy used in this study but with a different microstructure and investigated four predictive fretting fatigue parameters. He investigated the suitability of the Findley Parameter, Smith-Watson-Topper Parameter, the Shear Stress Range (SSR) Parameter and the Modified Shear Stress Range (MSSR) Parameter. He found that only the MSSR parameter was effective at predicting crack

location, crack initiation angle and fatigue life. Since the MSSR builds on the SSR, a brief overview will begin with the SSR parameter.

2.5.2 Shear Stress Range Parameter

This predictive parameter assumes that the stress range is affected by local mechanistic parameters located at the contact area. These include: peak contact area, local bulk stress, local shear stress, slip amplitude and contact semi-width. Iyer et al [12] found the stress range can be determined with the following formula:

$$\Delta\tau = \tau_{\max} - \tau_{\min} \qquad (2.19)$$

$\tau_{\max}$ and $\tau_{\min}$ are the shear stress values from the application of the maximum and minimum axial loadings. To find the stress range, the max shear stress range is found for all planes from -90° to 90° using equation (2.17) shown above. As can been seen by inspection, equation (2.17) does not take into account the effect of mean stress or stress ratio, both of which are documented in fatigue literature to be determining factors in fatigue strength. To remove this discrepancy, Walker [13] suggested an alternative method of finding SSR:

$$SSR = \Delta\tau_{crit} = \tau_{\max}(1 - R_{\tau})^{m} \qquad (2.20)$$

In the above equation , m is a fitting parameter chosen to collapse plain fatigue crack initiation data at different strain ratios. It has been shown to equal a value of 0.45 by Lykins [14]. R_τ is the stress ratio on the critical plane and is evaluated as:

$$R_\tau = \frac{\tau_{\min}}{\tau_{\max}} \qquad (2.21)$$

Madhi calculated the SRR parameter for IN-100 and found it did not meet the desired goals of finding the crack location, crack initiation angle and fatigue life with a high degree of accuracy.

2.5.3 Modified Shear Stress Range Parameter

The MSSR parameter is considered by many to be the premier predictive parameter of fretting fatigue behavior. This modified version of the SSR parameter takes into account the effect of the maximum normal stress and how it acts to open the crack surface. Namjoshi et al have shown that this parameter has also largely eliminated the effect of pad geometry on predictions from MSSR. It is calculated as:

$$MSSR = A\Delta\tau_{crit}^{B} + C\sigma_{\max}^{D} \qquad (2.22)$$

A, B, C and D are constants. For Ti 6Al 4V, Sabelkin et al [15] determined the constants to equal 0.75, 0.5, 0.75 and 0.5 respectively. Also for Ti 6Al 4V, Namjoshi showed that

the MSSR showed little dependence on the pad geometry. He also found the parameter can be used with an analysis to predict fretting fatigue life from plain fatigue life data. Further, he attributes the accuracy of MSSR to the use of both the shear stress and normal stress in the calculation. Like the SSR parameter, MSSR is found for all planes from -90° to 90° at all points along the contact line between the specimen and fretting pad. The critical plane is the plane where the MSSR parameter obtains a maximum. In this study, the MSSR parameter is calculated to check its accuracy compared to experimental fatigue life, crack location and crack initiation in IN-100.

2.6 Microstructure

The purpose of this section is to discuss the microstructure of the material used in this study. Since this material is heat treatment sensitive, and some work has been in the past to relate the material properties with specific microstructures, this section will outline some generalities found in the study as well as the microstructure used in this study. The material used is this study is IN-100. The material composition is in weight percent:

Al	Ti	Cr	Co	Mo	V	Fe	C	B	Zr	Ni
4.9	4.3	12.3	18.3	3.3	0.7	0.1	0.06	0.02	0.02	Bal

To produce this specific microstructure, a piece of IN-100 was obtained with the microstructure shown in Figure 2.3, and was subjected to: solution treat @

1121C/2hr/OQ, age @ 871C/40min/AC, stabilize @ 649C/24hr/AC and age @ 760C/4hr/AC to produce the microstructure shown in Figure 2.4. Inside the microstructure there are grains with an average size of 6 microns. (Milligan et al) [16] The large globular particles are Ni_3Al (Padula, Milligan et al.) [17] precipitates, in this case primary γ', the small globular particles found inside the grains are secondary γ'. These particles are very important in the behavior of this material. The precipitates are used to strengthen the material by impeding grain boundary slip. In the past, work has been done on correlating changes in microstructure to changes in strength for superalloys. Huther and Reppich [18] suggest the following formula for correlating strengthening mechanisms and material strength by calculating the change in the critical resolved shear stress:

$$\Delta\tau = \frac{1}{2}\left[1.62w\left(\frac{\Gamma}{b}\right)\left(\frac{Gb}{d_2}\right)f_2\right]^{\frac{1}{2}} \qquad (2.23)$$

With the following:

Γ =antiphase boundary energy

b= Burgers Vector

G=Shear Modulus

d_2 =Diameter of secondary γ' particles

f_2 = Fraction of secondary γ' particles

w=adjustable parameter to reflect dislocation shearing

In a given alloy system, the above equation can reduce to the following form:

$$\Delta\sigma \propto \left[\frac{f_2}{d_2}\right]^{\frac{1}{2}} \tag{2.24}$$

This model can be used to roughly estimate the strengthening effect of the secondary γ' particles. As can be seen, to increase strength, more secondary γ' with a smaller diameter will increase material strength. However, the above model does not take into account the effect of grain size. Milligan found that there was a correlation between strength and grain size, and the above equation needed a term to describe this effect on strength. Starting with a Hall-Petch relationship, Milligan determined the following term described the change in strength due to grain size (GS), $\left[GS\right]^{\frac{1}{2}}$. Or in total with the C_2 term equaling zero:

$$\sigma = \sigma_o + C_1\left[\frac{f_2}{d_2}\right]^{\frac{1}{2}} + C_2\left[d_3\right]^{\frac{1}{2}} + C_3\left[GS\right]^{-\frac{1}{2}} \tag{2.25}$$

It was also found by Milligan that larger secondary γ' particles resulted in a reduction in strain hardening, and the presence of primary γ' particles also decreases strain hardening. The effect of the primary and secondary γ' is especially noteworthy since

this is not the conventional relationship between strain hardening and precipitates. Milligan concluded in his study that there was a lack of grain size effect on strain hardening and the increase in secondary γ' size or the increased amount of primary γ' decreases strain hardening.

Jin and Mall [19] in a study on the effects of microstructure on short crack growth with a titanium alloy suggested that in alloys with similar material strengths, the differences in test data may lie in microstructure. Some of the conclusions drawn from this study showed that as a short crack grows from one grain size in length to several, the crack's growth is impeded by the number of changes in direction forced by changes in microstructure. The more changes, the slower the crack grows. It is well known that grain boundaries can serve as the most important impediments in crack growth, however in Jin and Mall's study, they suggest that the main impediment to crack growth were the Widmanstatten colonies inside the grains these were more important to crack growth than the grain boundaries. This suggests that short crack growth can be impeded by more than grain boundaries and the grain size is one among other factors determining short crack growth. In this study they concluded that a fine microstructure had better crack initiation resistance and a coarse microstructure had better crack propagation resistance.

Padula, Milligan et al. [17] in studied of the effect of grain size and precipitate distribution on the fatigue crack growth behavior of KM4 nickel-based super alloy, an alloy very similar to the IN-100 used in this study. The alloy was prepared in two ways for the test, solution treated above the γ' solvus temperature and solution treated just a

few degrees below the solvus temperature. The former super-solvus treatment made a large grain sized (55 micron for Padula's test) material, the later, sub-solvus heat treatment made a very fine (6 micron for Padula's test) grain sized material. The super-solvus material had a slightly higher percentage of γ' inside the grain boundaries, leaving less at the grain boundaries compared to the sub-solvus material. They found that the Paris slopes of the two materials were similar, however the sub-solvus material had a consistently higher fatigue crack propagation rate and a lower threshold. They also found considerably more tortuous crack path in the super-solvus material. Multiple reasons are referenced for the difference in behavior, including slip reversibility, increases in roughness-induced closure and deviation from the Mode I plane. Together, these factors lead to a reduced crack growth rate and increase the threshold of endurance strength with an increase in grain size. Finally Padula could not find a calculation method of ΔK_{1C} that matched his data even though a number of different approaches were used such as those used by Weertman [20], Lin and Fine [21], and Sadananda and Shahinian [22].

2.7 Previous Studies on Ni-Alloys

The study of nickel based alloys is currently in its infancy. Nickel based alloys can be monocrystalline or polycrystalline and studies have been done on both mono and polycrystalline alloys. Often these are quoted as starting points for work in nickel based super alloys such as the one used in this study. In fretting fatigue, extensive work has been done for polycrystalline titanium alloys and these have been used as direction for

this study. Several studies have been summarized in this section to show the current understanding and depth of study in nickel based alloys.

The first, done by Wan [23], used single crystal DD3 alloy at an elevated temperature to find a relationship between shear stress and cycles to failure in low cycle fatigue. Wan developed a model for experimental results and finite element analysis. He considered things such as mean stress effect and crystallographic theory in the analysis. In the theory he uses resolved shear stress (σ) and resolved shear strain of slip systems activated during fatigue cycles (τ^{α}). The following governing equation was developed:

$$\tau^{\alpha} = \sigma : P(\alpha) \qquad (2.26)$$

with:

$$P(\alpha) = 0.5(m^{\alpha} n^{\alpha^T} + n^{\alpha^T}) \qquad (2.27)$$

with α signifying the slip direction of the slip system and n^{α} and m^{α} as unit vectors normal to α.

To develop a relationship between shear stress and life to failure, a power law life model was assumed:

$$\frac{\Delta\tau_{\max}}{2} = AN_f^b \qquad (2.28)$$

In the above equation, $\frac{\Delta\tau_{\max}}{2}$ defines the maximum resolved shear stress amplitude of all activated slip systems. A and b are parameter and N_f is the fatigue life. This equation is only valid with a zero mean stress. However if mean stress is not zero the above equation is modified to:

$$\frac{\Delta\tau_{\max}}{2} = AN_f 1 - \left(\frac{\tau_m}{\tau_b}\right)^2 \qquad (2.29)$$

with τ_m defining the mean resolved shear stress on the slip system corresponding to the maximum shear stress and τ_b as the resolved shear stress corresponding to the ultimate tensile strength of the materal.

In a study by Shyam [24] a model for slip irreversibility on a polycrystalline nickel based super alloy deforming in a planar manner was developed. To begin a slip irreversibility parameter based on the fraction of dislocations existing on the free surface was developed. The parameter was given a scale from 0 to 1 with 0 equaling reversible slip and 1 equaling fully reversible slip. The test was a single stroke compression test with a variable of temperature applied for each test. The tests found slip irreversibility increased with temperature. Shyam concluded that since slip irreversibility increased

with temperature, this was the cause of a decrease in fatigue crack propagation threshold at increasing temperatures. Further, scanning electron microscopy showed deformation by slip acted on polycrystalline planes. The fracture surface was found to be on the octahedral slip plane (1 1 1) [0 1 1]. Shyam also found that the activation and movement of slip systems are the basic deformation mechanism of the notched and round specimens used for his testing.

Brien [25] tested the effect of microstructure on the characteristics of the single crystal nickel based super alloy AM1 at high temperatures for fatigue. Using repeated (below endurance strength) fatigue cycles, he found two types of fatigue based on microstructure, and from this a map of fatigue was constructed with two domains. The first was an anisotropic microstructure domain and it had a plastic behavior in fatigue unique to its microstructure. The second was a domain with a homogenous microstructure and it also had a plastic behavior in fatigue unique to its domain and dependent on microstructure.

Pierd [26] focused on creep fatigue crack growth in PM nickel based super alloy at high temperatures and high vacuum. He used various cohesive models and experimental data during his testing. The focus of the study was on the ΔK range with crack propagation during the reloading phase of creep only. Two simulations were used, one with a hold time and one without a hold time. He found that the fatigue and creep introduced damage fields were related to crack opening displacements introduced to the

specimens. He also found that predictive crack curves accurately reflect the influence of hold time duration during the reloading phase.

Sondhi [27] characterized the action of an internal stress field causing observed low or negative creep rates in tension for IN-100 tested in a pre-aged condition. Experiments showed an asymmetric response to creep with the initial creep in compression being slightly higher than in tension. This showed the existence of an internal stress field. In addition to characterizing his observations, Sondhi found it was possible to remove the asymmetry using thermal processes. He showed by testing the thermally processed specimens that the asymmetric response was removed.

Murphy [28] tested SCN specimens and IN-100 pads under elevated temperatures to find that a correlation between the fracture plane and the crystallographic plane existed. He found that the orientation of the material principal axes on subsurface stresses in significant. He also found the crystal orientations can be used to evaluate contact stresses and contact stresses can be used to find the cycles to failure. Finally he found that the fracture plane followed [1 1 1] to within a few degrees.

Madhi [11] did work very similar to the work undertaken for this thesis. The main difference was in grain structure and size, Madhi used IN-100 with a coarser, oblong grain size and structure than used for this study. Madhi's study used an IN-100 microstructure with a 10 micron by 50 micron oblong grain structure. This study uses a microstructure with a 7 micron circular grain structure. A comparison of the

microstructures can be found in Chapter 5 of this thesis. His study covered fretting fatigue at room temperature. He investigated the validity of extending predictive parameters from titanium alloys to nickel-based superalloys. He found the best parameter was the modified shear stress range parameter, the other three parameters investigated were not effective. He also investigated the validity of using the Ruiz program in violation of the b/a restriction. He found Ruiz gave an excellent approximation of the more accurate finite element approach.

The intent of this thesis is to continue to build a library of information on nickel based super alloys tested in room temperature under fretting fatigue conditions. As the above studies show, there is a lack of baseline knowledge for nickel based super alloys. This study will develop knowledge of polycrystalline nickel based alloys under fretting fatigue conditions. The study is done at room temperature to be used as baseline information for later studies introducing other variables to fretting fatigue such as the effects of temperature on the metals' behavior.

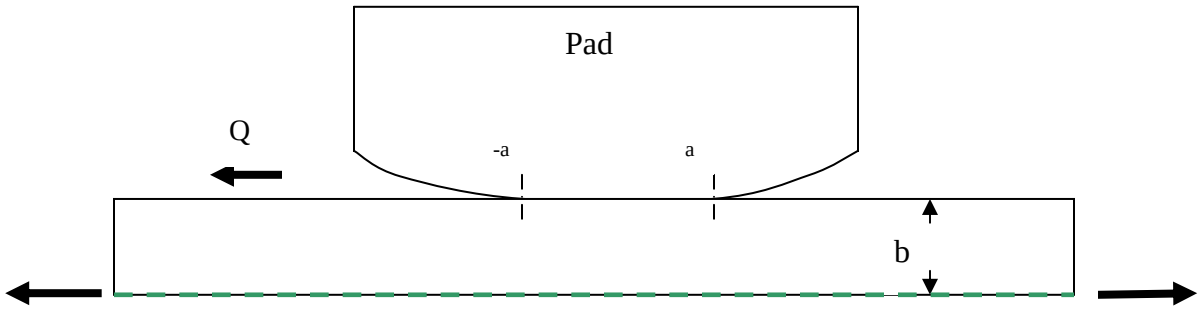

Figure 2.1 Fretting Fatigue Pad and Half Specimen

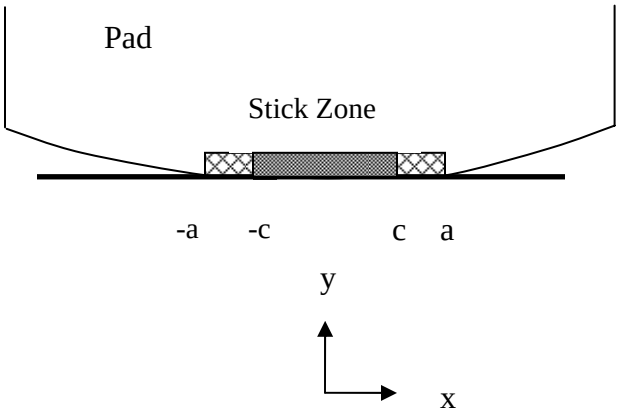

Figure 2.2 Stick Zone and Slip Zone

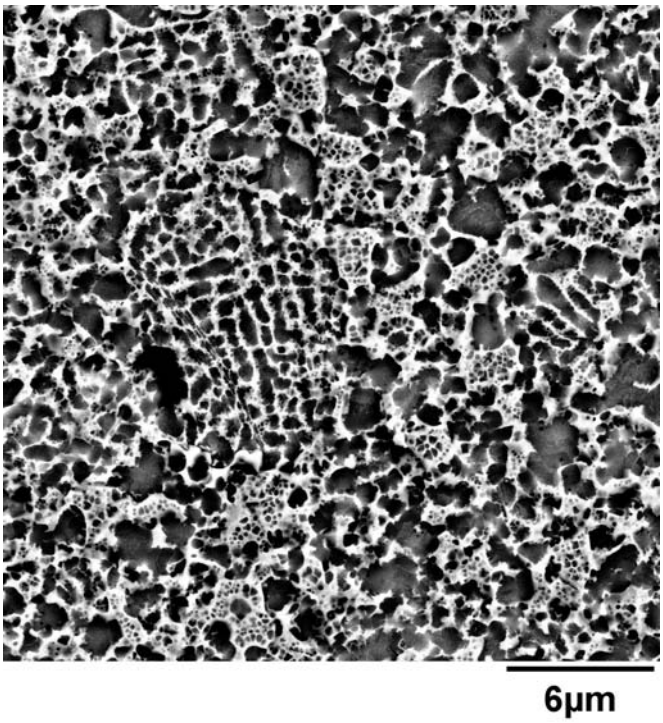

Figure 2.3 Microstructure before heat treatment

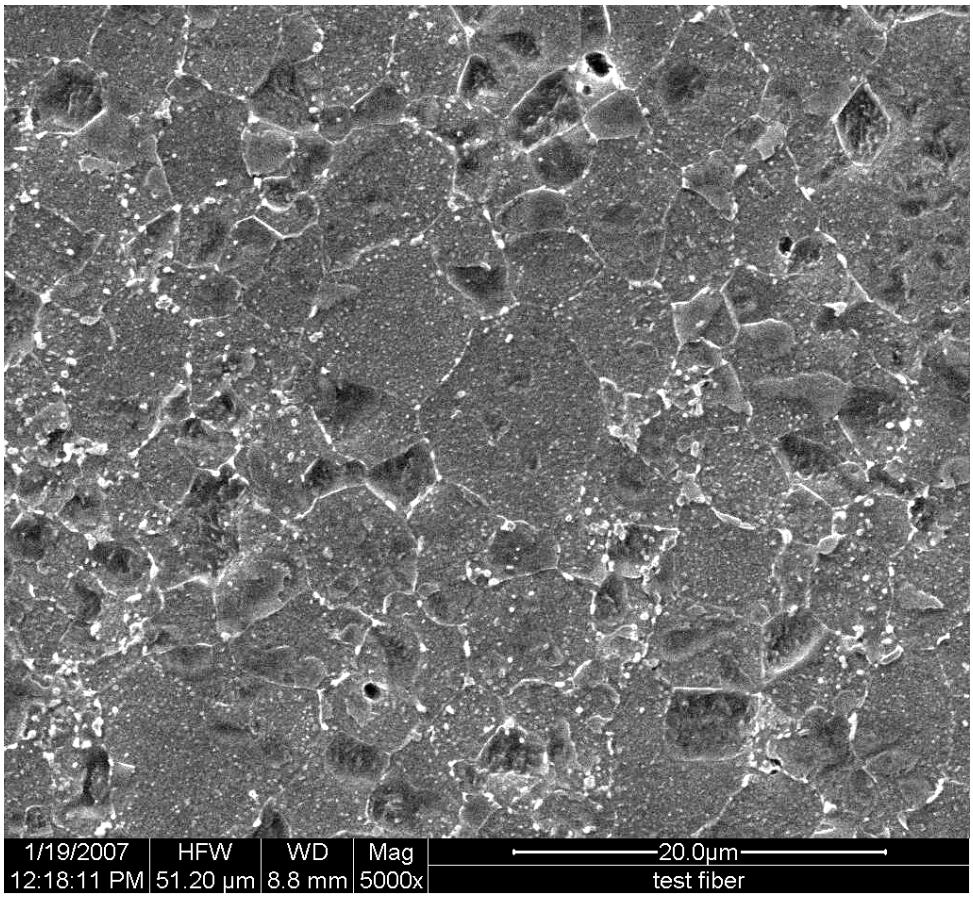

Figure 2.4 Microstructure after heat treatment

III. Method of Experimentation

The purpose of this chapter is to discuss the test design in detail. The test set-up is described with explanation of the equipment used and the procedure. The experimental configuration is described next, followed by the determination of the loads and frictional forces acting on the specimen. Finally, the crack development in the specimen is described.

3.1 Test Set-up

The test set-up can best be shown with a picture. Figure 3.1 depicts the actual machine used in experimentation. The material testing system is a 22.2 kN servo-hydraulic uniaxial test machine. The specimen is loaded into the load frame. The top of the load frame clamps onto the sample and holds the sample in place. A load cell measures the axial load needed to hold the sample in place. The bottom of the load frame is hydraulically activated and applies a cyclic load to the sample. The hydraulic actuator is controlled by a computer program named Multi-Purpose Testware (MPT). The variables loaded into MPT include the maximum and minimum magnitude of the cyclic load applied to the sample, the frequency of the load and the waveform of the load. MPT also has a ramp-up program used to bring the sample to the full cyclic test amplitude over a few seconds. The fretting load is applied via a spring loaded frame. The load is variable up to approximately 4500 N and is adjusted by threaded nuts on two parallel rods. Adjusting the nuts compress or decompress the springs to provide the desired load.

The spring load is recorded on two load cells one on each side of the frame. The fretting pads are mounted in the spring loaded frame and adjusted until a straight full contact is made with the tensile sample. The adjustments are made by using shims between the fretting pads and the spring loaded frame. The straightness of the contact between the fretting pad and the tensile sample is recorded with pressure sensitive paper (PSP). The shims are adjusted until the PSP indicates the contact between the fretting pad and the tensile sample is straight and even, giving an even amount of pressure on the sample from the fretting pads, one located on each side of the tensile sample. The specimen geometry is given in the following, see figure 3.2. The tensile sample is 127 mm, has a width of 6.35 mm and a thickness of 3.66 mm. The samples were specified to be made with a tolerance of +/- 0.0127 mm, most were well within this tolerance range however all were measured before testing and the actual dimensions were recorded. The fretting pads were 9.53 mm square and had a 50.8 mm radius on one end to contact the tensile sample, see figure 3.3. Both the specimens and pads are made of IN 100. The composition of IN 100 is described in the preceding chapter. The specimens have a grain size of 7 μm and the pads have a coarser grain size of 10 by 60 μm. The specimens and pads were fabricated with wire electrical discharge and finished with a grinder to a smooth surface. All sharp edges were removed and lightly rounded to avoid excessive stress risers in the test samples and for safe handling of all pieces.

3.2 Experimental Configuration

The intent of the experiment was to determine the S-N curve for both the fretting fatigue and plain fatigue of IN 100. A stress ratio of 0.03 is used to determine the maximum and minimum axial stresses applied to the samples, see Table 3.1. The following schematic shows the test configuration, see Figure 3.4, the specimen is loaded in to the load cell, the fretting pads, one at each side of the specimen are loaded into the spring loaded frame and as described above, the pads are aligned. The specimen is then loaded into the load frame and locked into place. The specimen is visually checked for proper alignment and adjusted if necessary. The program to run the specified test is loaded into MPT and prepared to run. The 4003 N fretting load is applied to the sample via the spring loaded frame and the MPT system is started. The software ramps the load up the maximum applied load. The system with the fretting load is allowed to settle for several minutes and then the lateral butterfly screws were then adjusted to finger tight plus one-quarter turn. This allowed the system to settle into a point of exactly the same load on each side of tensile sample and removed any side moment applied to the tensile sample. All the samples were run at 10Hz with a sinusoidal wave pattern. A peak valley compensator was used to reduce the variation between the command and feedback signals sensed and recorded by the machine. The axial loads and tangential loads were recorded at 0.04 second intervals on a log scale pattern. The loads were then recorded at 1…10, 100, 1000, etc. cycles up to failure of the sample. The number of cycles to failure was recorded and the output files were analyzed.

3.3 Load Determination

To determine the loads conditions in the tensile sample, two separate programs were used, one was an analytical method in a program called Ruiz, the second was a method based on Finite Element Analysis (FEA), both of these needed bulk and shear stress as inputs into the respective program. The axial (bulk) stress could be directly measured by the load cell, the shear stress however, needed to be calculated. The following formula was used to determine the shear stress, (V-W)/2=Q. V is the stress recorded by the bottom load cell, and W is the stress recorded by the top load cell. The difference of V-W is divided by 2 to determine the shear stress on each side of the tensile sample. Therefore, Q represents the shear stress on one side of the tensile sample. To determine if the fretting condition was met by the test, several graphs have been made using Q and several other variables. Q versus axial stress is graphed, to meet the requirement of fretting, this graph must settle into a hysteresis loop see figure 3.5. Usually, for at least the first 500 cycles, the tensile sample and fretting pads are in a condition of gross slip, not producing a hysteresis loop, but the test should settle into a fretting condition by 1000 cycles. The second graph that can be made shows the Q_{max} and Q_{min} versus the number of cycles. The Q values should stabilize with time, showing a steady value of Q_{max} and Q_{min} until failure of the sample, see figure 3.6.

3.4 Determination of Coefficient of Friction

To use the FEM program, the coefficient of friction is needed as an input variable. This particular variable was not specifically determined for this study, but was instead used from previous studies. It has been shown that the coefficient of friction will stabilize within 1000 – 2000 cycles of the beginning of the test. To determine the coefficient of friction, a contact load was applied to a sample held at one end and left free at the other, the load was increased until a condition of gross slip developed between the fretting pads and tensile sample. The coefficient of friction was then calculated from:

$$f=Q/P$$

The coefficient of friction, f, stabilized from 0.35 to 0.45. For this study, the value of 0.45 was adapted for the analytical and FEM work.

3.5 Crack Development

In fretting fatigue, crack development is very important. It needs to have a certain initiation point and also it needs to follow a certain orientation. Because the crack needs to develop in accordance to these criteria, the crack initiation location can be predicted. The crack needs to initiate at or near the trailing edge of contact between a fretting pad and the tensile sample see figure 3.7. The half contact width can be observed from the broken tensile sample. Ruiz and the FEM program can predict the half contact width

from the loads, coefficient of friction and geometrical information about the sample. Scanning Electron Microscope (SEM) can be used to determine the crack orientation and crack initiation zone. To do this, the specimen is sawed laterally along the x-axis at the center of the crack initiation zone. Once the cut sample is polished, the SEM allows a view of the crack orientation. These angles and locations can be compared to the FEM predictions for the crack.

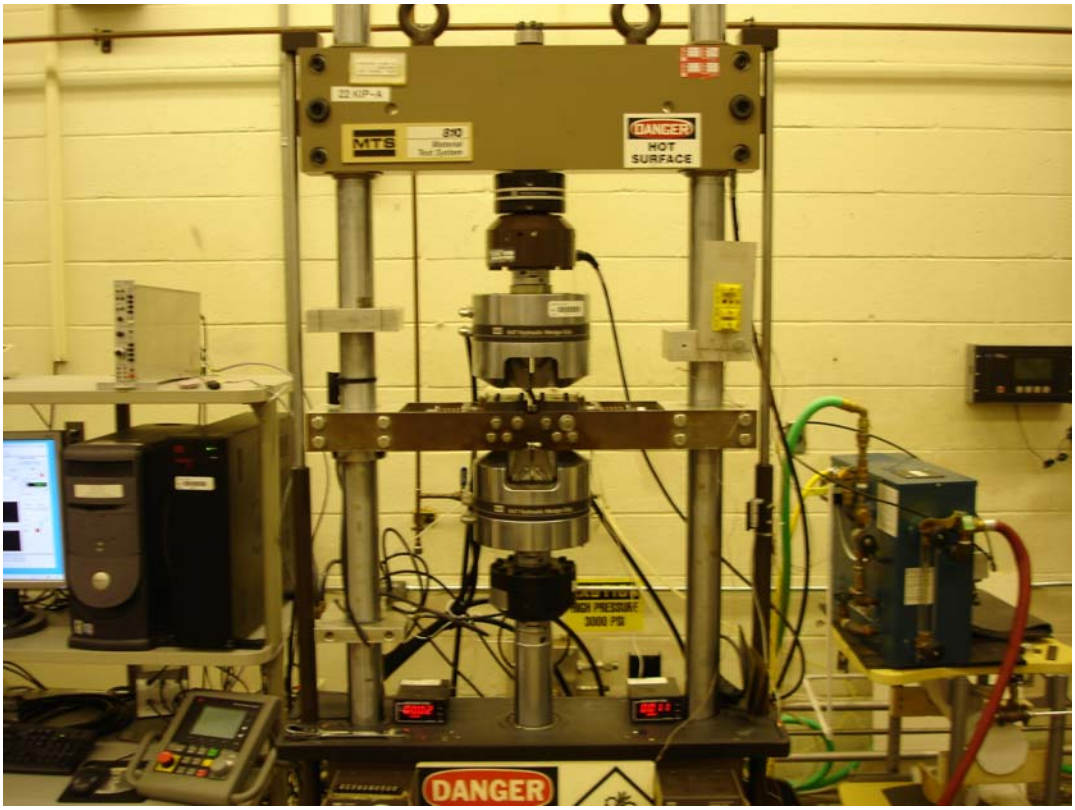

Figure 3.1 Test Apparatus

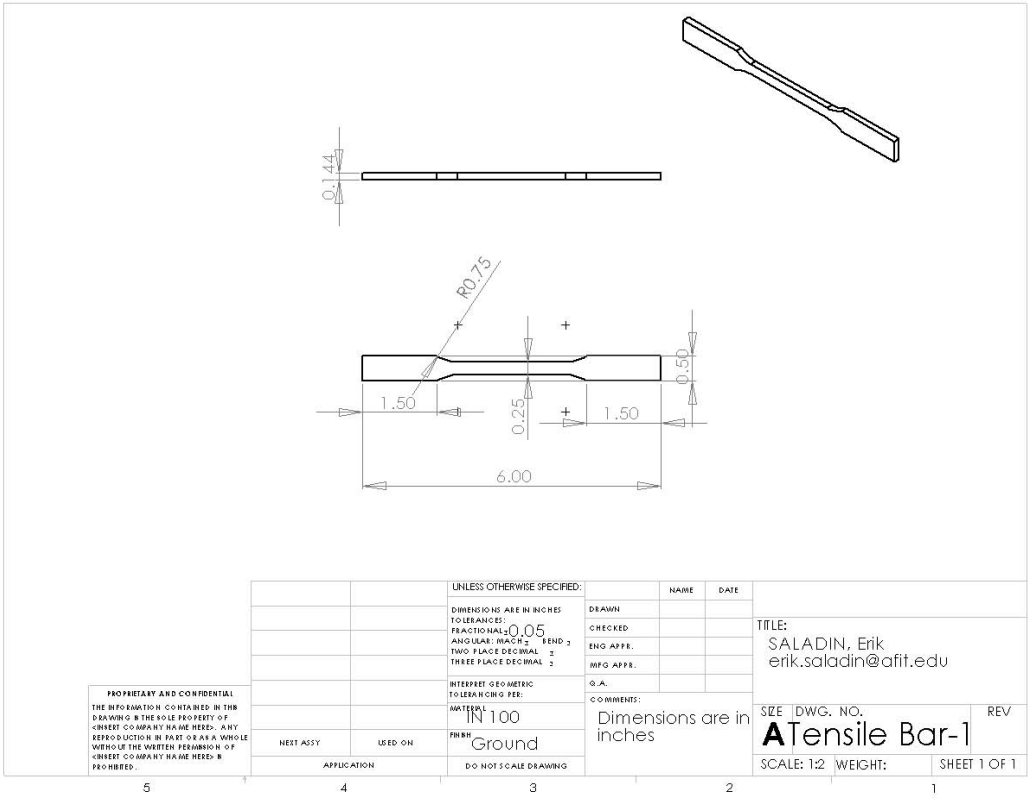

Figure 3.2 Specimen Dimensions

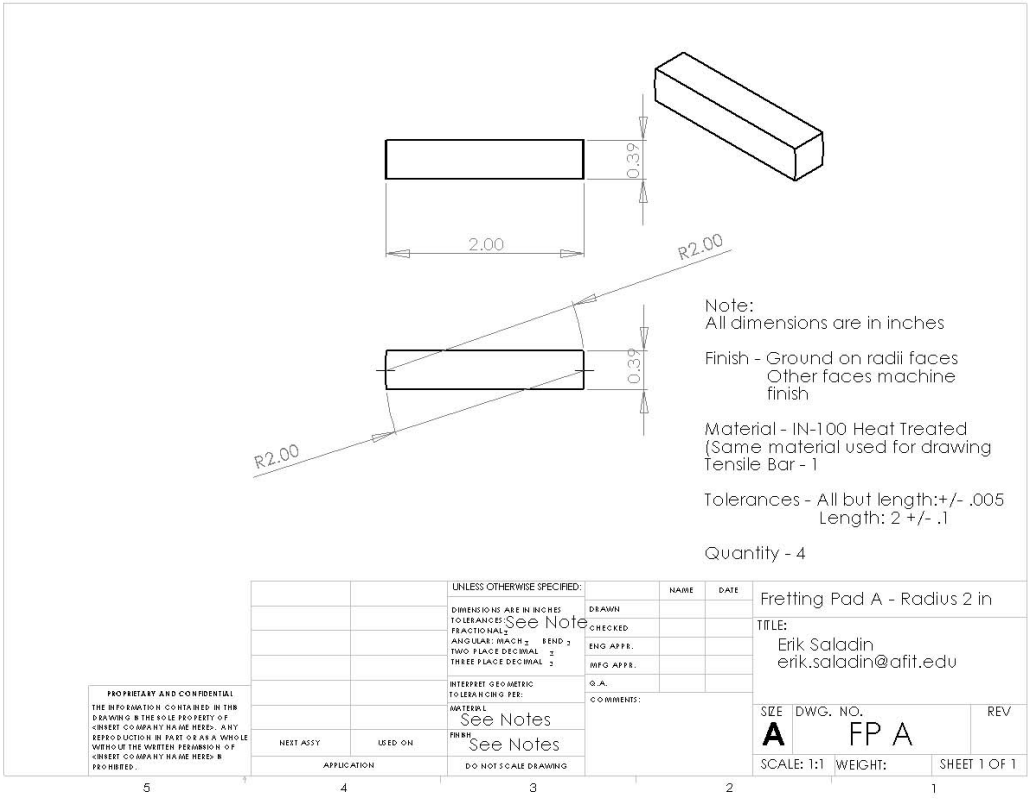

Figure 3.3 Pad Dimensions

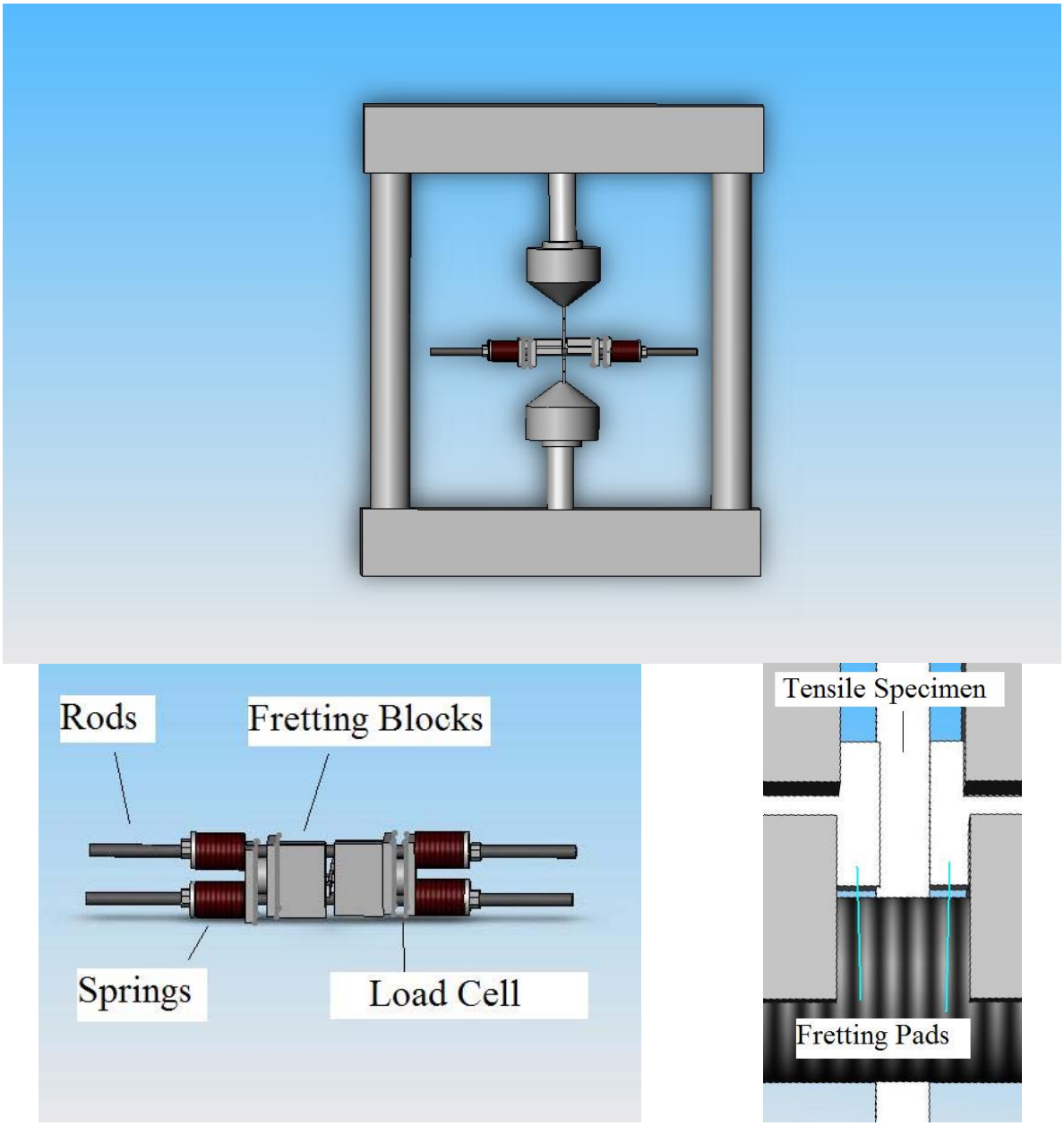

Figure 3.4 Schematic of Test Apparatus

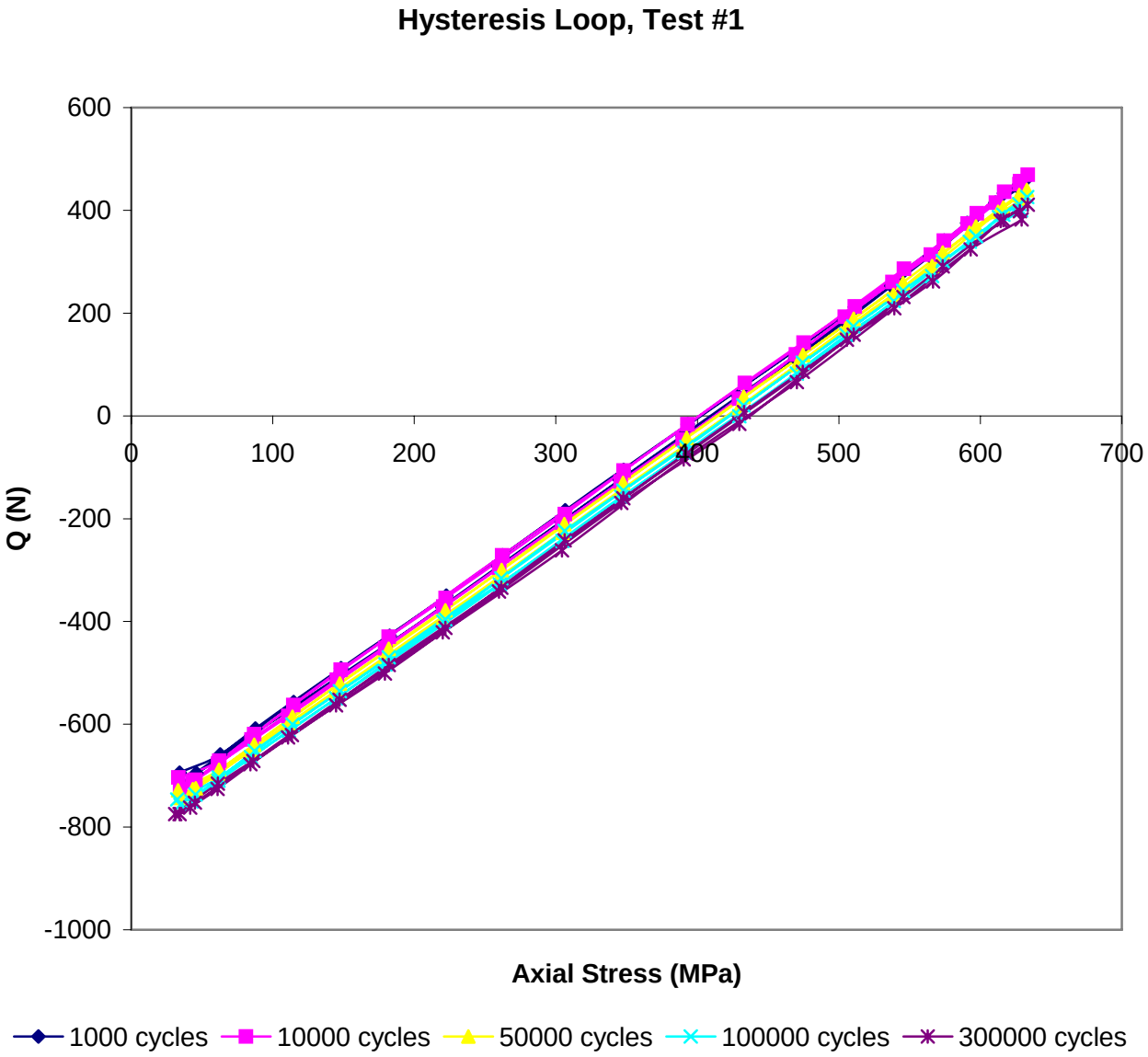

Figure 3.5 Hysteresis Loop

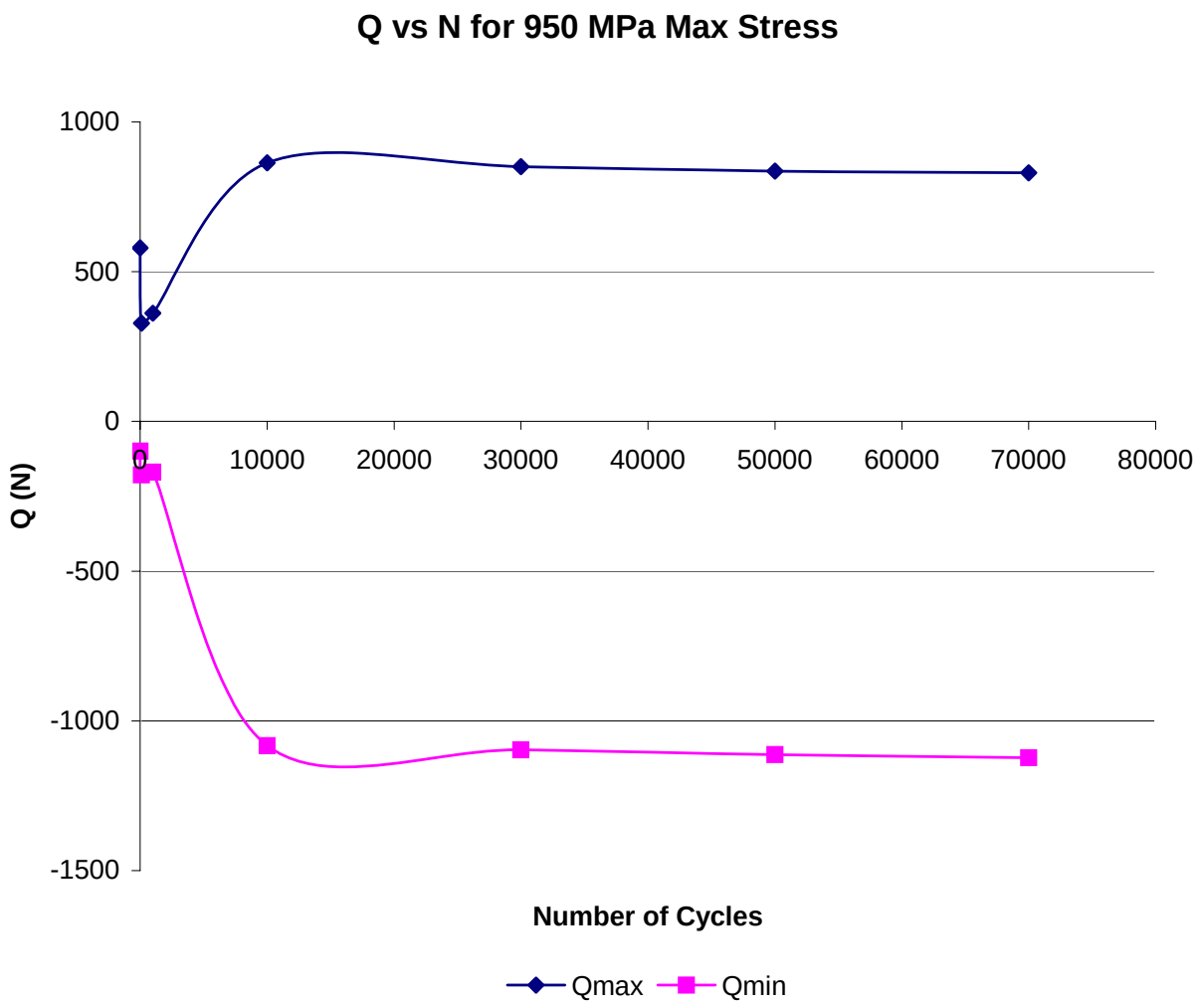

Figure 3.6 Q_{max} and Q_{min} versus Number of Cycles

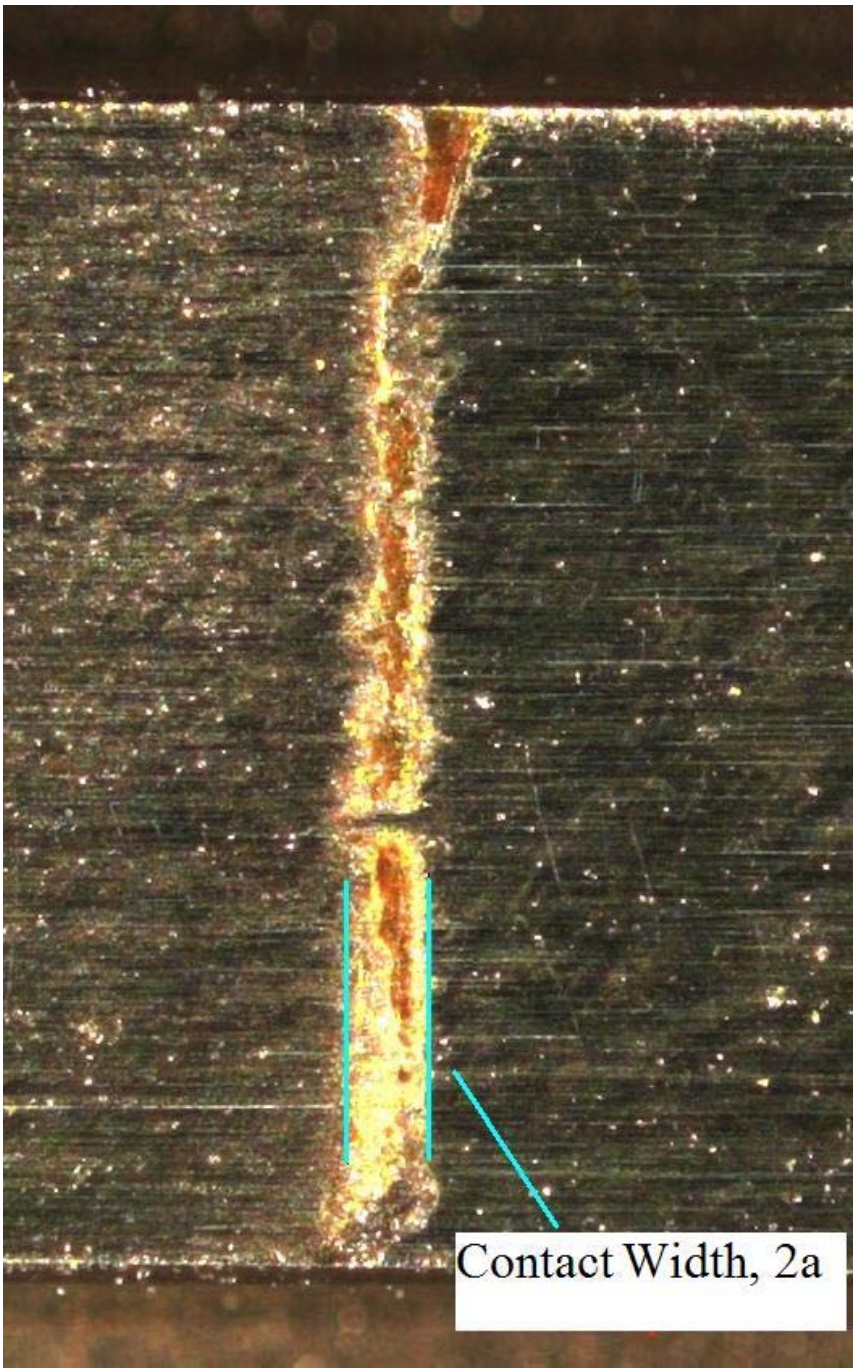

Figure 3.7 Scar View

Table 3.1 Experimental Test Settings

Test	Type	Pad	P	Stress	Stress	$\Delta\sigma$	σ_{eff}
		mm	N	Max(MPa)	Min(MPa)	MPa	MPa
1	Fretting Fatigue	50.8	4003	550.00	16.50	533.50	542.51
2	Fretting Fatigue	50.8	4003	600.00	18.00	582.00	591.83
3	Fretting Fatigue	50.8	4003	650.00	19.50	630.50	641.15
4	Fretting Fatigue	50.8	4003	750.00	22.50	727.50	739.79
5	Fretting Fatigue	50.8	4003	800.00	24.00	776.00	789.11
6	Fretting Fatigue	50.8	4003	950.00	28.50	921.50	937.07
7	Fatigue			600.00	18.00	582.00	591.83
8	Fatigue			650.00	19.50	630.50	641.15
9	Fatigue			800.00	24.00	776.00	789.11
10	Fatigue			1050.00	31.50	1018.50	1035.71

IV. Finite Element Analysis

This chapter will address the use of finite element analysis (FEA) to model the fretting fatigue process for the specific parameters used for this study. First, the requirements of FEA will be addressed, and then a description of the model configuration will be given. Next the load inputs will be discussed and finally a brief comparison of the Ruiz output with FEA's output will be discussed.

4.1 Requirements of FEA

The model used for FEA is discussed in this section, including the mathematics of the model; the advantages of FEA compared to other analytical and test measuring, and the approach used by FEA.

The model used in the FEA program is based on the cylinder on flat configuration. In this model, the tensile bar specimen is modeled as being flat and the fretting pads are modeled as cylinders. The tensile bar is situated between the two cylinders; each cylinder carries a constant load pressing on the tensile bar. Previous studies have indicated that the contact area is dependant on the applied load. The contact load is defined as in equation 2.6 and as the equation shows, takes a hertzian shape. The FEA method does not depend on the half-space assumption and therefore can be used regardless of the ratio of b/a. In the case of this study, the half-space assumption, b/a>10

has been violated so the analytical approach taken by the Ruiz method is a useful estimation but does not have the best accuracy In the case of this test, b/a=3.02.

The FEA program uses the following approach to finding the contact half-width:

$$a = \sqrt{\frac{2PA'}{k\pi}} \qquad (4.1)$$

In the above equation, P is defined as the normal load applied to the tensile bar specimen and A' is defined in terms of material properties:

$$A' = \frac{4(1-\upsilon^2)}{E} \qquad (4.2)$$

with the following definitions, E=modulus of elasticity and υ = possion's ratio.

Also, the radius of curvature is defined as:

$$k = \frac{1}{R_1} + \frac{1}{R_2} \qquad (4.3)$$

Hills [29] has shown that violating the half-space assumption can cause a deviation in the expected results. Since the FEA solution does not require a relationship between a and b, FEA can give better results than the analytical method discussed in chapter two.

4.2 FEA Advantages

Finite element analysis has many advantages over other solution methods including analytical and the experimental solutions. The first important advantage is the ability to give a solution without regard to the relationship of b and a, also known as the half-space assumption. FEA can also find a number of local parameter that allow for the direct solving the solution outlined in chapter two. These parameters are: p, a, $\delta_{\max}$, $\tau_{x,\max}$, $\Delta\tau_{x,\max}$, $\sigma_{x,\max}$, $\Delta\sigma_{x,\max}$ and can be found from the boundary conditions and the following loads and stresses, P, $\sigma_{xx,\max}$, $\sigma_{xx,\min}$, $Q_{\max}$ and $Q_{\min}$. The FEA model can also show the tensile stress concentration on the tensile bar specimen from the applied contact load only. This is something unique that can't be accomplished in any other way (12). The FEA method can also be used to show that contact semi-width is not necessarily symmetric around the center of contact Magaziner [30]. Since FEA offers these advantages, it has been chosen for this study.

4.3 FEA Approach

The finite element method uses a unique approach to solve problems. In FEA, the elasticity of the body is used as a way to solve the problem. Strain energy is stored in the body as potential energy and this relationship is used to solve the problem. FEA is done by taking a continuous body and dividing it into an n x n set of nodes. The governing

equations deriving from the relation between potential energy and elasticity are applied to the nodes to determine stress, strain and displacement. In this approach, a large equation set is created and solved simultaneously. For this case, four node plane strain quadrilateral elements are used to find the stress, strain and displacement magnitude at the contact interface. ABAQUS is used to solve a Chemkin input file. The contact conditions are simulated with a master and slave interfacial algorithm. In this configuration, the master surface has anchor points located by drawing unit vectors from the slave surface nodes to the master surface. The slave nodes then deform relative to the anchor points.

4.4 Description of Model

The model used is a two dimensional representation of the test set-up with a permanent pad radius of 50.8 mm. The model consists of three parts, the tensile specimen acting as a slave surface, a fretting pad, as a master surface, and a rigid body constraint. Since the test set-up is symmetrical, the model only simulates one-half of the test set-up, see Figure 4.1. The ABAQUS algorithm determines which segments on the master surface interact with the slave surface. The contact algorithm is established from the master slave node relationship and the algorithm determines how loads are transferred at the contact surface. The bodies have numerous constraints applied to them to simulate the test set-up. To constrain the tensile specimen it is fixed in the negative x-direction in the simulation. This partly simulates the clamped end of the test set-up. The tensile specimen is allowed to roll in the x-direction and the top end of the tensile specimen is

free to move. Since the model only simulates half of the test set-up, the model's tensile test specimen is 1.83 mm thick. The length of the specimen is 9.53 mm in each direction from the center of contact with the fretting pad simulation, see Figure 4.1. The pad is fixed in the x and y directions however the pad holder is allowed to roll in the y direction. The pad and tensile bar specimen have a multi-point constraint (MPC) so neither body can rotate due the applied loads. The pads are also constrained to the top nodes of the pad so they move in unison. The borders of the pads and specimen use a multi-point constraint to keep the border elements from penetrating each other during simulations, see Figure 4.2. The pad and tensile bar specimen have the properties of IN-100 and the pad holder is deliberately given a low value of E, (5 MPa) and a poisson's ratio of 0.3, these values ensure a lack of interaction between the pad and the holder. The loads used in the simulation are of three types. The first is a contact load applied to the upper side of the pad. The second is a tangential load applied at the left side of the half-space of the model. The third is an axial stress applied at the right side of the tensile bar specimen. In addition, there is a small sliding contact condition applied between the pad and tensile bar specimen. The mesh in the model uses a four node plain strain elements. This type is used to avoid oscillation in the stress state along the contact surfaces, other meshes would not work as well for this oscillation reduction. The pad and tensile bar specimen meshing become finer towards the center of contact between the pad and specimen. This change is made to give the best stress, strain and displacement definition at the area of contact and to reduce computation time at the less important areas far from the contact area. The coefficient of friction for the computation is 0.45, a smaller number would not allow a converging solution.

To run a simulation of an experimental test, two computations must be done. Each computation is done in two steps; the first is to apply the constant contact load to the model, the second is to find the corresponding bulk stress point and the corresponding value of Q. The first computation is to find the maximum Q and bulk stress and the second to find the minimum Q and bulk stress. In the first computation the 4003 N constant contact load is applied and the maximum load conditions are simulated, this would be the finite element analysis of the tensile bar specimen with the peak load applied to it and the maximum shear force applied to the tensile bar specimen, see Figure 4.3. The second computation simulates the minimum load, 3% of the maximum load applied to the tensile bar specimen. In this condition the shear force in the tensile bar is at a maximum in the opposite direction. During this simulation the constant contact load remains at 4003 N, see Figure 4.4.

4.5 Model Validation

The finite element model used in this investigation can be checked with the Ruiz results. The output from Ruiz is normalized based on hertzian peak pressure and frictional coefficient and the output from the FEA program are in pounds per square inch. To compare the results, first the FEA output will be normalized using the hertzian peak pressure and frictional output from the Ruiz program. Next the Ruiz outputs will be converted to Megapascals (MPa), and compared to the FEA output, also converted to

MPa. By converting the FEA output to the Ruiz output and then vice versa, the conversion factors can be eliminated as a source of error in the graphs.

The converted graphs should show a reasonable amount of accuracy between the two calculation methods despite the violation of the half space assumption in the Ruiz calculation. Please see Figure 4.5 to see a comparison of the stress profiles both solutions converted to MPa. To analytically check the two models against each other, the contact half-width, the hertzian peak pressure and nominal stresses can be compared for each solution.

4.5.1 FEA and Ruiz Comparison

To compare the FEA output to the output of Ruiz, the FEA output has been normalized using the friction and hertzian peak pressure estimates from Ruiz. We can see that the stress profile of the normalized S11 ($=\sigma_{xx}$) output from FEA is similar to the output of Ruiz, see Figure 4.6. Further, in converting both the FEA and Ruiz outputs to MPa and comparing it can be seen that the profiles are the same as in the normalized graph but on a different scale, see Figure 4.7.

4.5.2 Peak Pressure and Contact Half-Width

The peak pressure, S22 ($=\sigma_{yy}$) in the FEA model will be checked against the peak pressure found in the Ruiz model at the x/a=0 point. In Ruiz, the peak pressure is -725 MPa. The peak pressure found in the FEA program is -660 MPa. This gives a difference of 8.9%.

4.5.3 Stress Profiles

The stress profiles maximums and positions were recorded for S11, S22 and S12 ($=\sigma_{xy}$) in both FEA and Ruiz. These values were then calculated as a percent difference of each other. The following table shows the results:

	S11		S22		S12	
	Max	Position	Max	Position	Max	Position
	MPa	x/a	MPa	x/a	MPa	x/a
Ruiz	950	1.04	-725	0	-295	0.4
FEA	1060.2	0.969	-658.8	-0.0315	-279	0.4343
Difference	10.40%	6.80%	9.10%	1.60%	5.40%	7.90%

As can be seen above, all the stress maximums are within 11% and the positions are within 8%, this effect is due to the violation of the half space assumption. The profile shapes of S11, S22 and S12 for Ruiz and the FEA program are similar and are shown in figures 4.7, 4.8 and 4.9. It can be seen that Ruiz and FEA results show good agreement.

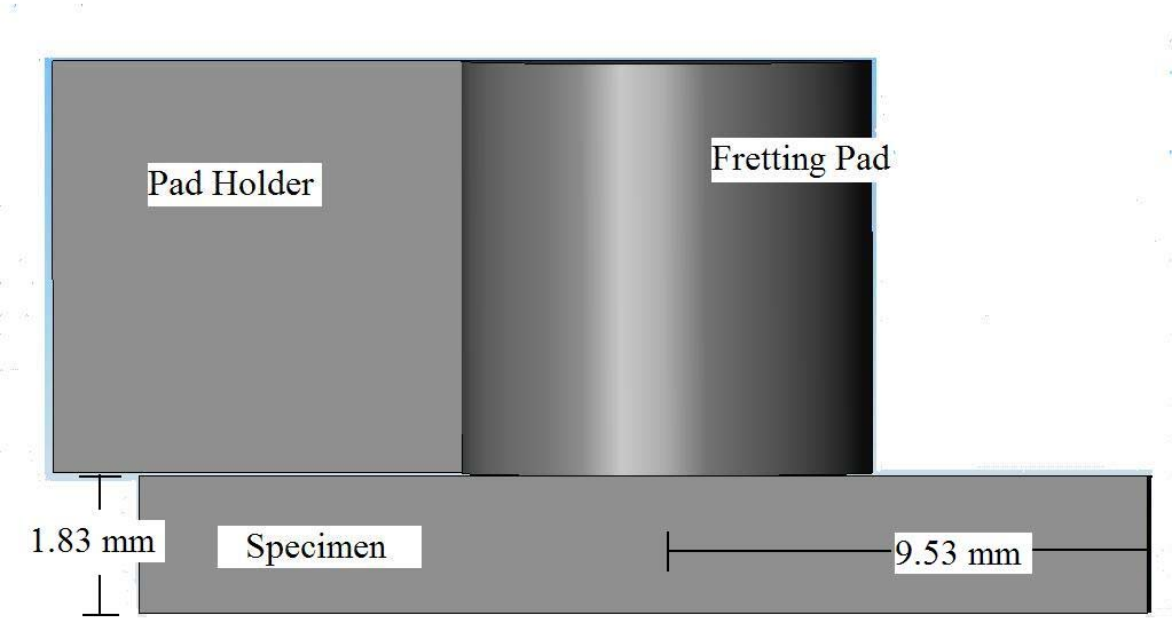

Figure 4.1 Finite element model

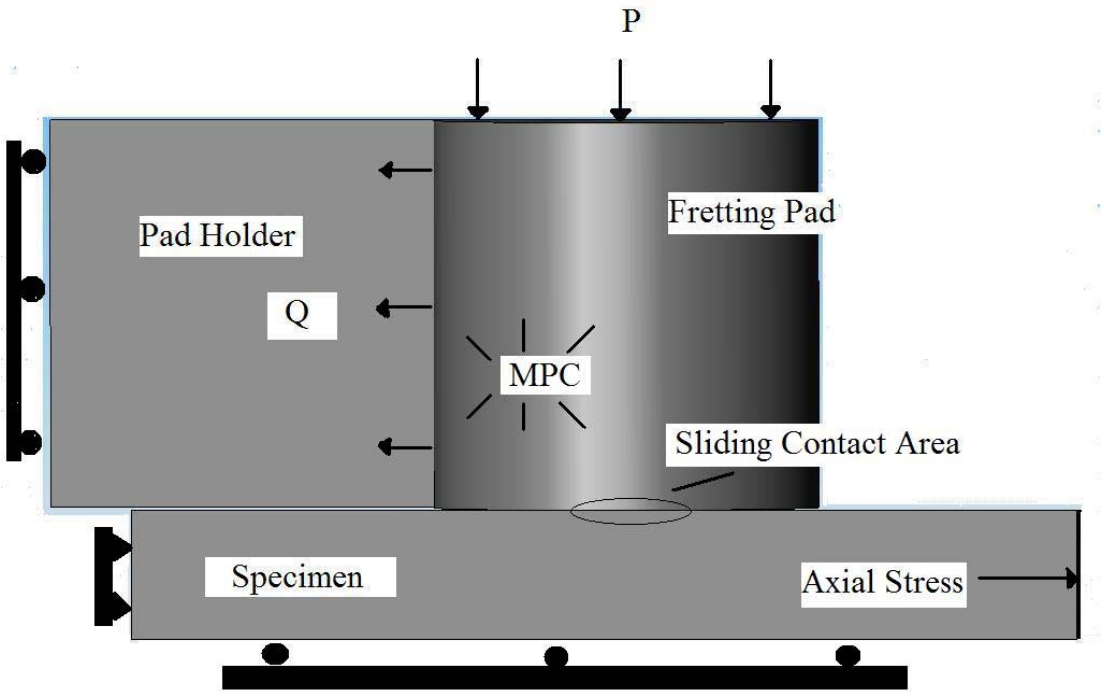

Figure 4.2 Constraints and loads for the finite element model

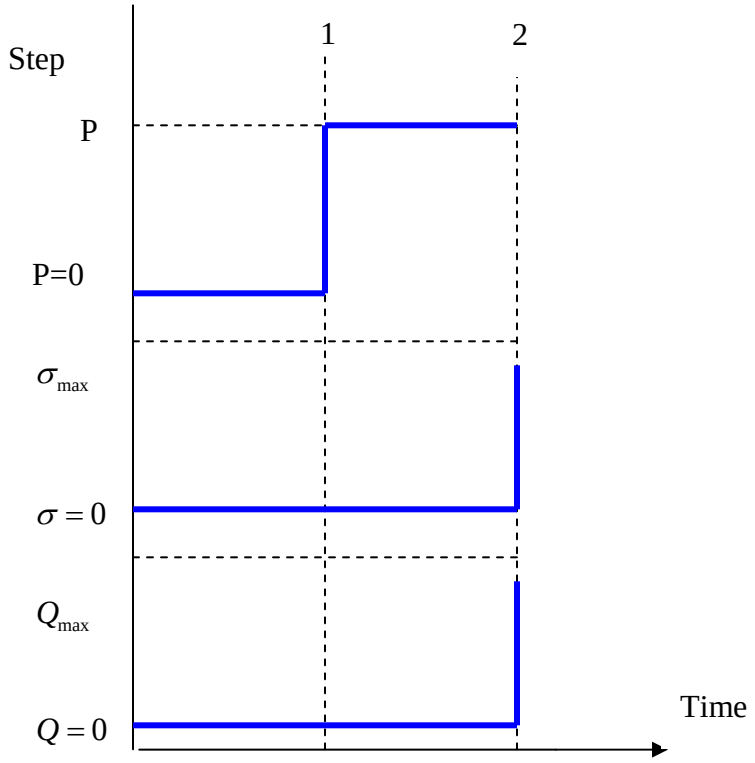

Figure 4.3 Step application of load for maximum fatigue cycle condition

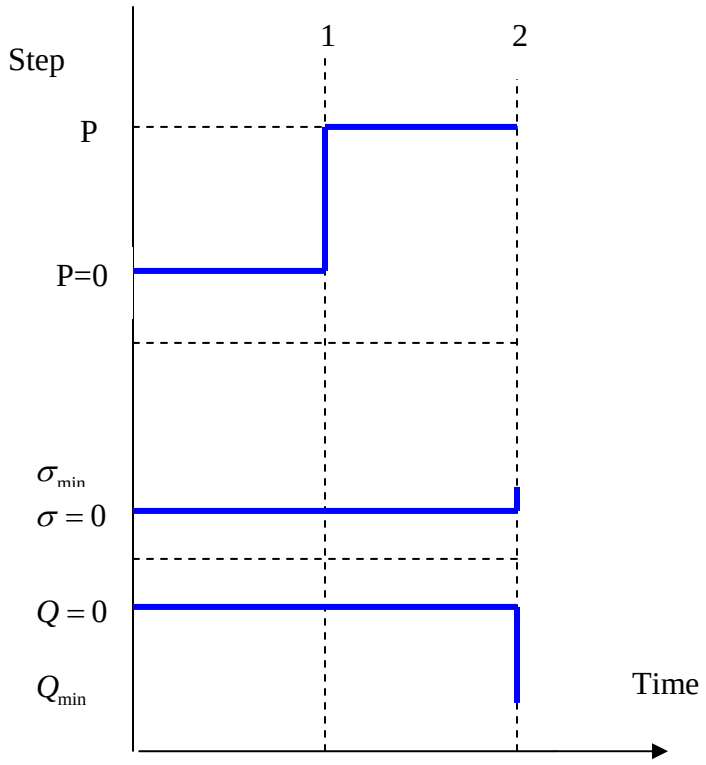

Figure 4.4 Step application of load for minimum fatigue cycle condition

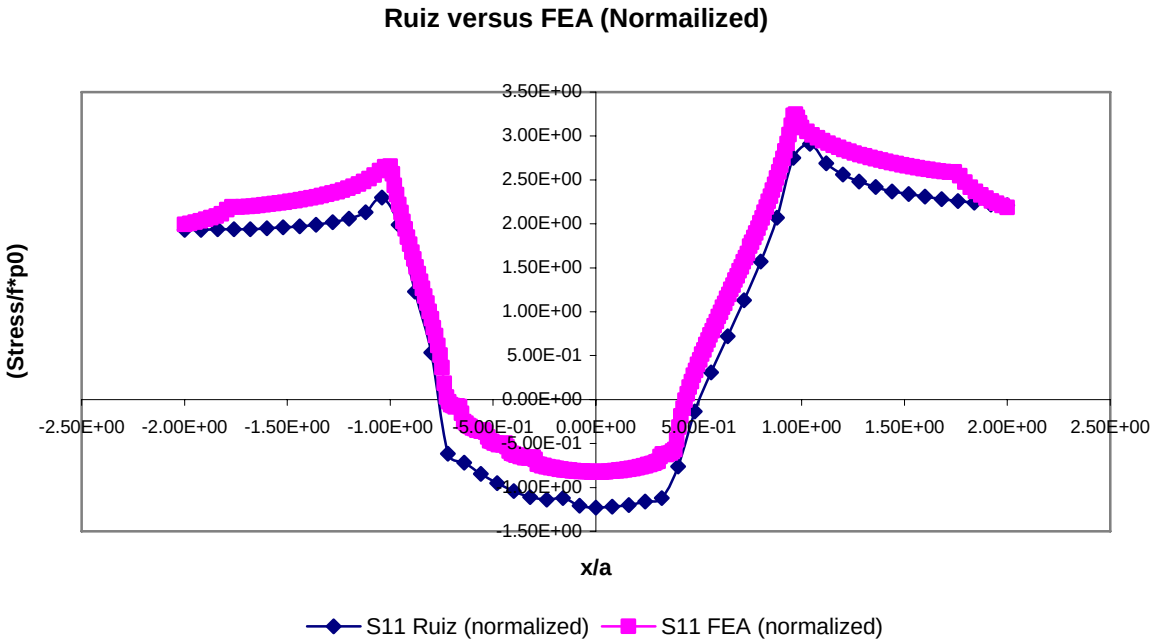

Figure 4.5 Normalized longitudinal tensile stress, S11

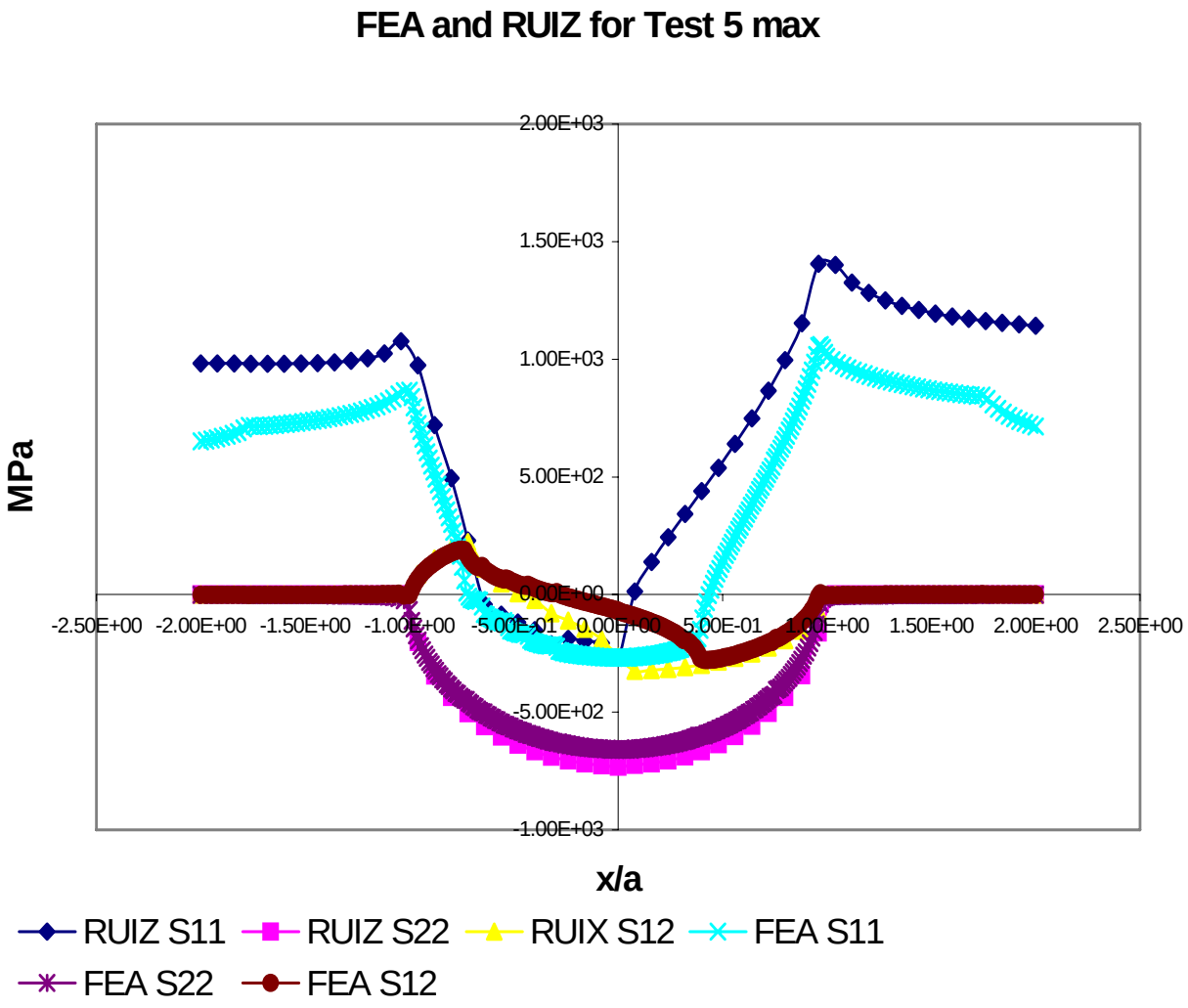

Figure 4.6 Comparison of stress components from FEM and Ruiz

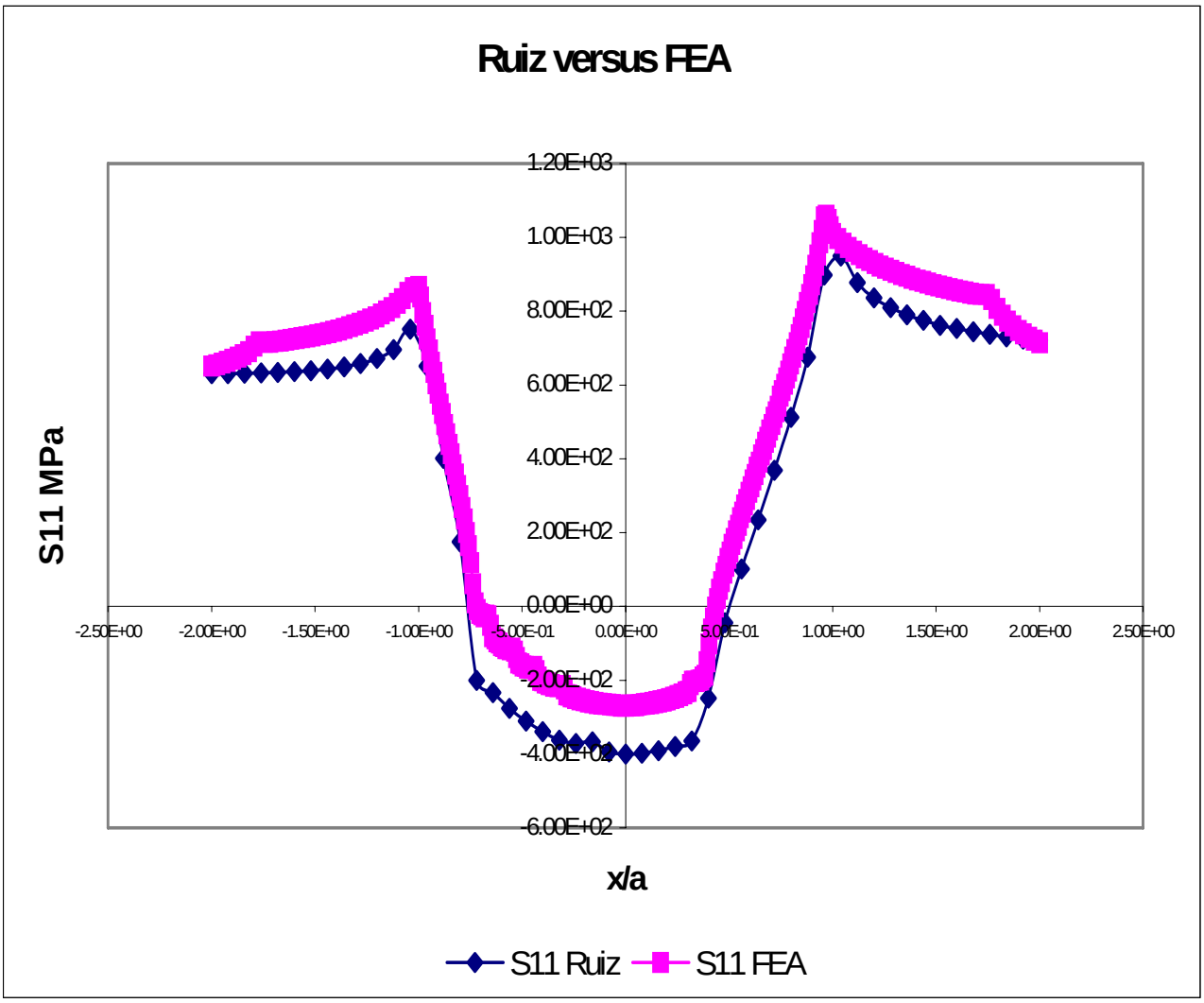

Figure 4.7 Comparison of S11, longitudinal stress from Ruiz and FEA

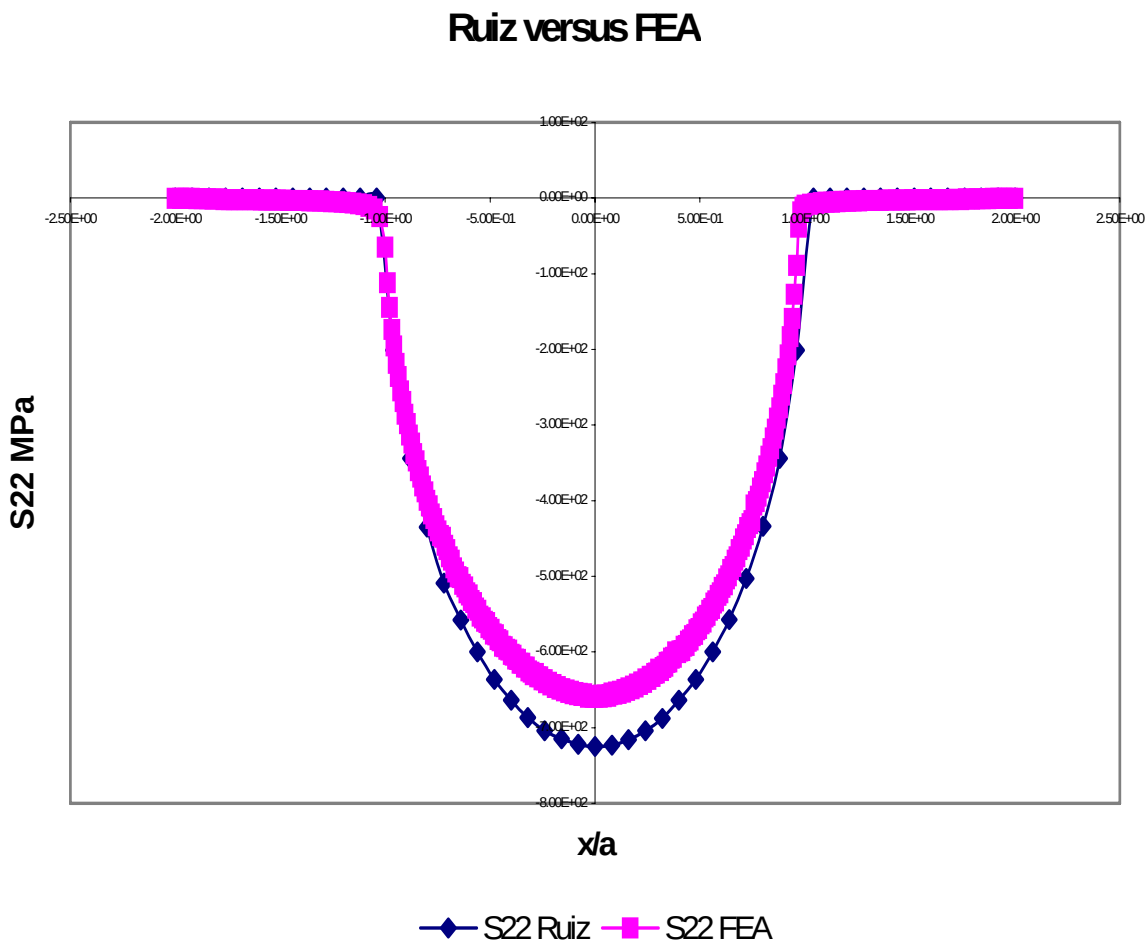

Figure 4.8 Comparison of S22, transverse stress from Ruiz and FEA

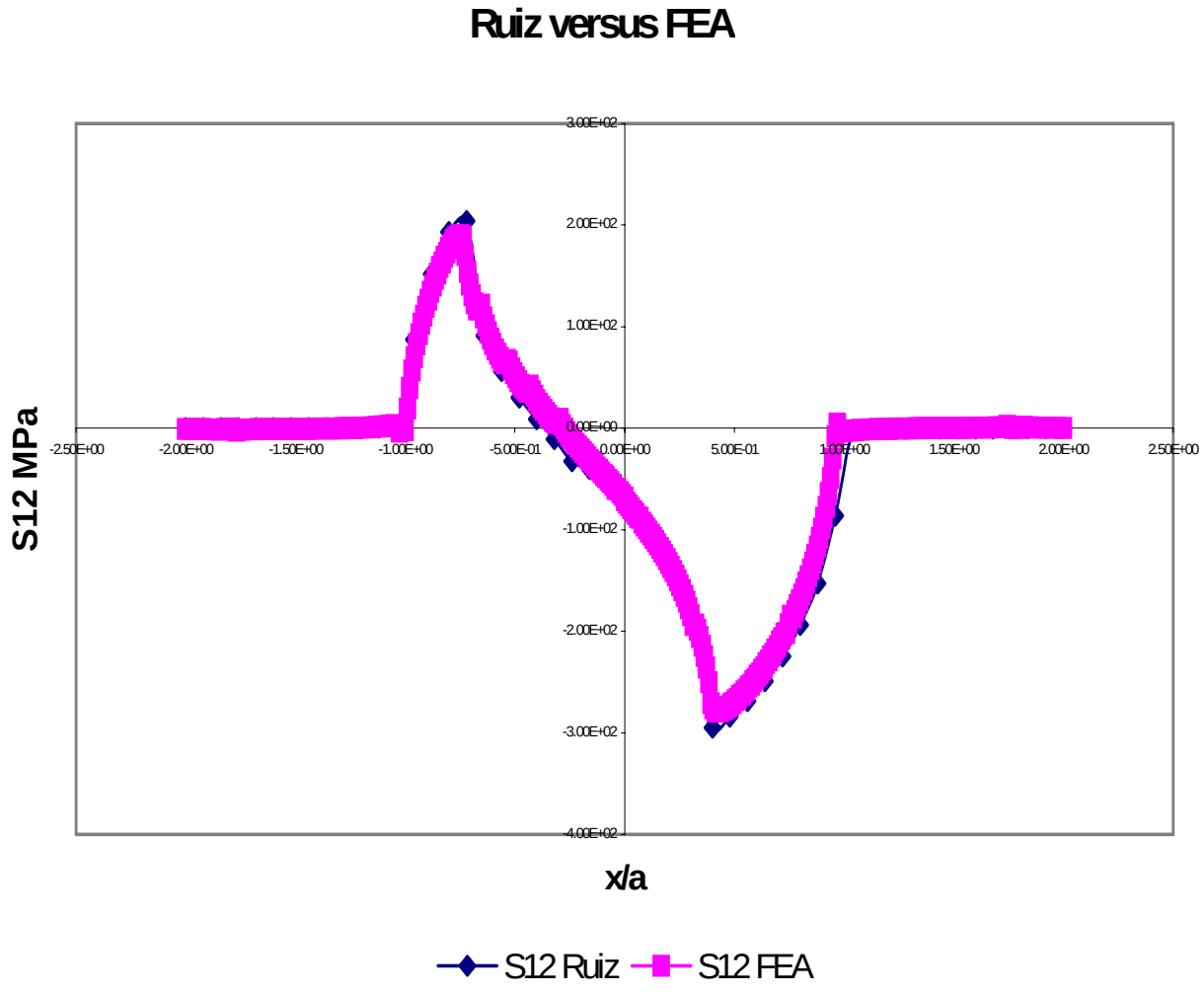

Figure 4.9 Comparison of S12, shear stress from Ruiz and FEA

V. Results and Discussion

This chapter will cover five general topics. The first is a presentation of the data, discussing the tests done, cycles to failure of the tests and the resulting S-N curves. The second is to evaluate if the fretting condition was achieved by evaluation of the data. Third, computational data will be measured against experimental data and evaluated for consistency and accuracy. Fourth, the microstructure of the material will be discussed and using a second different microstructure of IN-100, the materials will be compared in fretting fatigue. Some conclusions will be drawn about how the microstructure is affecting the S-N data from each. Finally, the conclusions of this test will be used to determine if the behavior of IN-100 with respect to microstructure in fretting fatigue is similar enough to high strength titanium alloy behavior to extend the fretting fatigue work from titanium into nickel-based superalloys.

5.1 Experimental Results

The experiments were conducted in both fretting fatigue and plain fatigue for a range of different maximum stresses. The R-ratio of the maximum and minimum stress was maintained at 0.03 for all tests, see Table 5.1. The table shows as the cycles to failure, N_f increases the change in stress, $\Delta\sigma$ decreases. Two tests were inconclusive, test #4 even though fretted, broke below the fretting scar for an unknown reason. Test #7 broke very early in testing, about 600,000 cycles, and is not used because it is inconsistent with the rest of the data.

5.1. 1 Evaluation of Fretting Fatigue Condition

Several different tests are used to evaluate if the fretting fatigue condition has been met. In fretting, Q, as defined in section 3.3, can be plotted against the applied stress. Within 500 cycles of the beginning of the test, the data should fall into a hysteresis loop. By inspection of Figure 5.1, it can be seen that a hysteresis loop had developed by 500 cycles. Once the hysteresis loop is established, it is maintained for the remainder of the test, see Figure 5.2. A second method is used to establish if the fretting condition has been met, the maximum and minimum value of Q must establish and maintain a value for the duration of the test, see Figure 5.3. and 5.4. In Figure 5.3, a maximum Q value is of 600 MPa is met at 50000 cycles and maintained for the duration of the test. The minimum Q value of -1100 MPa is met at 50000 cycles and maintained for the duration of the test. In Figure 5.4, it is can be seen that the maximum and minimum Q values become steady much earlier at 10000 cycles and had values of 900 and -1100 MPa, respectfully.

5.1.2 Fretting and Plain Fatigue Data Comparison

Stress versus cycles to failure curves are plotted for both the fretting and plain fatigue conditions in the following, Figure 5.5. It shows the fretting fatigue curve has a very aggressive upward turn in the fretting fatigue cycle at about 650 MPa maximum stress. The plain fatigue S-N curve begins an aggressive upward curve at the same

maximum stress level, but at about a 35% increase in cycles to failure, see Table 5.2. The plain fatigue curve offers a 35% increase in cycles to failure for a given stress level over the fretting fatigue condition over the range tested, see Table 5.2. This shows that fretting causes a substantial decrease in cycles to failure for IN-100 for this fine 7 micron grain sized microstructure.

5.1.3 Fracture Surface Area

The fracture surface area shows three distinct areas as the specimen progressed from crack initiation, linear crack growth and finally fracture as the applied stress equals the strength of the cracked specimen. In Figure 5.6, three separate areas of crack development are shown. Area one shows the initiation area of the crack, showing debris and wear. The second area shows the area of crack propagation. Notice the smoother appearance of this area. The third region shows deep dimples and surface distortion of the final fracture.

5.1.4 Crack Initiation Location

In fretting fatigue it is common to see the point of crack initiation along the trailing edge of the fretting specimen with respect to the fretting pad at the boundary of the stick zone. Magaziner (30) suggests this is caused by the fretting motion causing the boundary of the stick zone to move slightly, causing an area of very high stress. Since the trailing edge of the test specimen is the point of highest applied axial stress, any crack

initiated at this point would be in a position to continue to have a very high applied stress during crack propagation and growth to ultimate failure. On the samples used in this test, this boundary point is at x/a=+1. In all the tests, this was at or very near the point of crack initiation. In Figure 5.7, the dark area designated as the crack initiation area has a very aggressive crack angle and is accompanied by wear induced deposits of oxided material within the crack area and surrounding the crack area.

5.1.5 Half Contact Width

Half contact width equations 4.1 to 4.4 show that contact width is defined by three variables, the applied load P, the material properties and the radius of curvature of the specimen and pad. All of these variables are constant for each test, showing that the half contact width for each test should be exactly the same. In Table 5.3, it can be seen that the half contact widths measured had very good agreement with the half contact width values calculated by the Ruiz program. All values show agreement within 12.1 percent. It noticeable as the axial loading increased on the specimens, the error between the measured and calculated half widths increased, however overall the agreement is very good. It should also be noted that the half contact width is very difficult to measure. The exact half width can be difficult to find and on a broken piece, often only a small portion is left undamaged and complete after the breakage, usually on the side opposite of the crack initiation point.

Ruiz was able to accurately predict the half contact width, even though the half-space assumption was ignored. This shows the Ruiz calculation method can be used for IN-100 fretting fatigue samples with the same dimensions as used in this study without regard for the half-space assumption. However, it does not suggest the half-space assumption can be ignored in all cases.

5.1.6 Crack Initiation Orientation

Currently, there has only been a small amount of work done concerning nickel-based superalloys and fretting fatigue crack initiation angles. However, there has been a larger amount of work done on titanium alloys. In Ti-6Al-4V, it has been shown that the crack initiation angle is $45° \pm 15°$ (15), (30). Madhi (14) experimented with determining if the initiation angle in IN-100 was similar to titanium. Mahdi found that the initiation angles in his material were very similar to the angles found in titanium alloys. In this study the crack initiation angle was found for a sample to evaluate if it also would be similar to the initiation angles found by Madhi. To accomplish this, first a picture of a broken piece with an optical microscope was taken, and then the crack initiation point was identified from the picture. Usually, several or more cracks will start, but only the crack that propagated is of interest. The end of the sample is cut and mounted, then ground down to the crack initiation point. The crack initiation point was estimated to be 2 mm from the end of sample, and the sample was ground to this depth, measured with a set of calipers. Once at the proper depth, a picture was taken of the sample and the angle

was measured, see Figure 5.8. As can be seen in the Figure 5.8, the crack initiation angle was 40 degrees.

5.2 Computational Data

Two types of computational data were generated for this study. First, the Ruiz program was used based on an analytical solution. Secondly, a finite element approach was used to generate a solution. In chapter four, the two solutions are shown to be in good agreement. Ruiz was used to generate the MSSR parameter solutions outlined in chapter two. Madhi (14) evaluated the effect of changing the MSSR parameters, A, B, C and D and did not find this had a significant effect on the outcome of the results. For this study, the MSSR parameters given in chapter two are used without modification. As can be seen in Table 5.4, the MSSR parameter agrees well with the test data. Every sample broke at the trailing edge, as can be seen; the MSSR parameter predicted this with excellent accuracy. The MSSR parameter predicted a location of x/a=.96, very close to the trailing edge of the contact area defined as $0.89<x/a<0.99$. The crack initiation angle was measured for test #4, and was found to be 40° compared to the predicted angle of 25°, leaving 15° of error between the predicted angle and the experimentally found angle.

Next, the MSSR parameter was evaluated to determine the effect of fretting fatigue on the MSSR parameter versus plain fatigue. As can be seen in Figure 5.9, the effect of fretting was to increase the MSSR parameter for the fine microstructure versus the fine microstructure plain fatigue data; it can also be seen in Figure 5.9, that the two

data plots maintain a nearly linear relationship with an 18% difference from 70,000 to 1,000,000 cycles. It is very unusual for fretting fatigue to increase the MSSR value versus plain fatigue, however only three plain fatigue tests were taken and it has been shown in studies such as (10) that there can be a considerable range in MSSR data. It was shown in (10) that MSSR data taken for 50.8 mm fretting pads could be higher than the plain fatigue data. However, in Madhi's study (14), it was shown by adjusting the MSSR constants to A=0.5, B=0.25, C=0.75 and D=0.5, fretting fatigue data using 50.8 mm radius pads dropped below plain fatigue data, for the coarse microstructure of IN-100 used for comparison with the fine microstructure IN-100 used in this study. This pattern is more consistent with MSSR data taken for titanium alloys such as (10). Figure 5.9 also shows the MSSR results of Mahdi (14) for a coarse microstructure in fretting and plain fatigue, the data for this coarse microstructure is also shown in Table 5.5. The coarse microstructure fretting data is above the plain fatigue data. However, the MSSR parameter for fine and coarse microstructured IN-100 collapse well onto the same the same graph. The difference in MSSR is more pronounced in the high cycle fatigue region versus the low cycle to fatigue region, but the difference is never more than 9% in the high cycle to fatigue region. This suggests that MSSR can be used to predict cycles to fatigue independent of microstructure in IN-100.

Finally, the MSSR parameter was evaluated compared to Ti-6Al-4V. Fretting and plain fatigue data is shown in Figure 5.10 for IN-100 in a fine and coarse microstructure and also Ti-6Al-4V all fretted with 50.8 mm fretting pads. As can be seen, the difference in the data is a 35-43% increase in MSSR for the IN-100 versus the titanium alloy data.

It is intuitive to see the IN-100 material have a higher MSSR curve since the IN-100 material in both microstructures is considerably higher strength than the Ti-6Al-4V alloy. The MSSR parameter does not take into account the tensile strength difference between these two materials and since it does not, the curve may be too high or too low. This suggests the MSSR parameter has potential for IN-100, however, the parameter has been shown to be more effective with modified constants. This suggests, developing a new set of constants for IN-100 would be a fruitful area of study.

5.3 Microstructural Effects on Fretting Fatigue in IN-100

This thesis section is devoted to evaluating the effects of microstructure on the fretting fatigue phenomenon. First, the microstructure used in this study will be discussed, discussing the grain size and shape, precipitate distribution and size. A discussion of the effect of this microstructure on fatigue will be discussed, extending data from a fatigue study on a similar nickel-based superalloy, KM4. Next, a discussion of a different microstructure of IN-100 will be introduced, discussing the material's grain and precipitate sizes and shapes. Fretting fatigue data has been collected for this material in the same range as used in this study. The two will be compared and conclusions will be made about the microstructural affects.

5.3.1 Fine grained IN-100

In this study, a fine grained IN-100 alloy was used. The material was heat treated to produce an average grain size of 7 microns and round grain structure. The primary γ' have been allowed to move toward the grain boundaries with very little γ' left inside the grains. A secondary γ' has been allowed to develop and evenly propagate inside the grain boundaries. Precipitates are often used as a strengthening mechanism in high temperature application metals, see Figure 5.11. In a fatigue study by Padula (21) on a material very similar to IN-100, the following observations were made about fatigue behavior and grain size. As the grain size was made finer, ΔK_{th} was lowered, the crack growth rate, da/dN increased relative to a larger grained material subject to the same ΔK, the smallest possible crack size at initiation increased, the non-linear, early crack propagation rate increased as well as the linear crack growth rate. It was also found that the crack growth was more planar, showing little deviation in path as it grew. However, the fine grain sized material had a higher tensile and ultimate strength. In equation 2.25, it is shown that material strength is also affected by precipitate size and quantity, however, Padula did not find an association between precipitates and fatigue characteristics.

5.3.2 Coarse grained IN-100

In a previous study by Madhi (14), a coarse grained IN-100 alloy was used. The material was heat treated to produce oblong grains, averaging 10 microns wide and 50 microns long. The primary γ' have not been allowed to move as much to the grain boundaries, retaining some of the primary γ' inside the grain boundaries. Since tensile and ultimate strength is dependent on grain size and precipitate size and distribution, coarse grained nickel-based superalloys generally have a lower strength. As shown by Padula, the grain size affects the fatigue characteristics of the material. Since the grains in this material are an oblong shape, this suggests the material has some directional fatigue characteristics, see Figure 5.12. Since the grains are difficult to see, four grains are outlined to show size and proportion.

5.3.3 Comparison of two IN-100 microstructures in fretting fatigue

It has been found that in fretting fatigue that 90-95% of the life of the specimen is spent in crack nucleation and propagation up to a detectable size (~0.1-0.2mm) (31). Since the tensile specimen starts in the pristine condition, the majority of the test is spent in crack nucleation and early propagation. For this reason, fretting fatigue is largely dependent on a materials ability to resist crack initiation. On a fretting fatigue curve, the most initiation dependent data is in the high cycle fatigue range. The influences of crack propagation become more prominent in the lower cycle fatigue data. Figure 5.13 shows

the coarse microstructure shows more cycles to failure compared to the fine microstructure for the same stress range. This shows that the coarse microstructure has better crack initiation resistance compared to the fine microstructure. A survey of the early propagation rates of cracks in fine and coarse nickel-based superalloys in Table 5.6 suggests the slower crack growth and higher crack initiation threshold of the coarse structure may be reasons for this difference. For Ti-6Al-4V, Mall, Namjoshi and Porter (31) suggested the slower early crack growth rate in a fine microstructure of the titanium explained the same phenomenon noted for a coarse microstructure on IN-100 by this author. In the lower cycle to fatigue part of the curve, the data appears to collapse together. Since in this part of the curve, crack propagation is more influential in the total cycles to failure, this suggests the crack propagation behaviors of the two microstructures are similar but not entirely identical. Note the coarse microstructure's curve always stays to the right of the fine microstructure's curve. In Table 5.6, since the crack propagation rate in non-linear propagation (see early propagation rate column) and linear crack growth is always slower in the coarse microstructure, this would explain the positioning of the two curves. Also, in a plain fatigue comparison of a fine and coarse microstructure IN-100, the coarse microstructures slower crack growth rate and higher ΔK_{th} would explain the positioning of the coarse structures curve higher and to the right of the fine structures curve, see Figure 5.14. It also shows if crack propagation is a stronger influence the curves become more similar and if removed, would suggest a coarse microstructure has better crack initiation resistance. Figure 5.15 shows the fretting and plain fatigue curves together for both microstructures. As can be shown, the coarse data curves are higher than the fine curves, however the difference is about

5.4 Relevance on titanium alloys

Much of the background work in fretting fatigue used in this study was originally developed on titanium alloys. To develop an understanding of how these materials differ and are similar, one of the objectives of this study was to evaluate if the influence of microstructure in IN-100 is similar to the influence of microstructure on titanium alloys such as Ti-6Al-4V and Ti6242. First, a short overview of the effects of microstructure on fretting fatigue for Ti-6Al-4V will be given. The overview will be followed by a discussion of the similarities and differences between the behavior of Ti-6Al-4V and IN-100 in fretting fatigue due to microstructure.

5.4.1 Overview of titanium alloy behavior in fretting fatigue

As stated above, in fretting fatigue 90-95% of the total life to failure is spent in crack nucleation and very early propagation. Mall, Namjoshi and Porter (31) used a study of short crack growth in Ti6242 by Jin and Mall (19), to explain the behavior of Ti-6Al-4V in fretting fatigue. The effect of microstructure on fretting fatigue behavior in Ti6242 follows the size of the grains in the material, but even more so, the α / β lamellae colony size within the grains are effective at changing the crack initiation and early crack growth. A finer microstructure lowered the ΔK_{th} and slowed the early crack propagation rate. The crack growth was more planar, however the lower threshold da / dN decreased relative to a coarser grain size. The early crack propagation rate is slower, however once

crack development moves into the linear regime, the crack growth rate is similar without a strong dependence on grain size. As the grain size is increased for Ti6242, the ΔK_{th}, becomes higher, the crack propagation rate, da/dN becomes greater, the crack growth becomes more tortuous and the lower threshold da/dN becomes higher. The early (non-linear) crack propagation rate is faster and then resembles the fine microstructure's linear crack growth rate. The changes in crack growth due to microstructure are summed in Table 5.7 and more information is given in Appendix C. A quick survey of Tables 5.6 and 5.7 together shows the grain size is affecting the crack growth behavior of titanium alloys differently than the nickel-based superalloy IN-100.

5.4.2 Comparison of IN-100 and Titanium alloys in fretting fatigue

Several differences and similarities can be drawn between IN-100 and titanium alloys. A survey of Table 5.6 and 5.7 shows there are differences and similarities in the fundamental fatigue behaviors of the materials as microstructure is changed. In the IN-100 material, the test data shown in Figure 5.13 shows crack initiation has a dependence on microstructure. In the titanium alloy Ti-6Al-4V, the crack initiation resistance decreased as the grain and Widmanstatten colony size increased (31). In the IN-100 material, the smallest microstructural unit affecting fatigue is the grain size. Precipitates are not acting to change the fatigue characteristics. In the titanium alloy, both grain size and Widmanstatten colony size is affecting the fatigue behavior. This is a significant change in fatigue behavior between the two materials. In the titanium alloy microstructure plays a role in crack initiation and in IN-100 the results of this study

indicate microstructure also play a role. During crack growth periods, IN-100 shows a faster non-linear crack propagation rate and linear crack propagation rate with a decreasing grain size. Also as the grain size decreases the initiation crack size increases. In Ti-6Al-4V, it has behaved in an opposite manner compared to the IN-100 in the above measures. A finer microstructure decreases the crack growth rate, da/dN and the early propagation of the crack is slower with a decrease in grain size. The linear crack growth rate is much less dependent on microstructure. However, in other ways IN-100 and Ti-6Al-4V behave in a similar manner. In both materials, reducing grain size reduced ΔK_{th}, and the crack growth became more planar.

For IN-100 subjected to fretting fatigue, crack initiation appears to be best resisted by the coarse microstructure. It appears the microstructure is a significant factor in why the coarse microstructure has enhanced fretting fatigue resistance. In Ti-6Al-4V, a fine microstructure showed enhanced fretting fatigue resistance and the slower short crack growth rate of the fine microstructure compared to coarser microstructures was suggested as a reason. In IN-100, it is possible the coarse microstructure has a slower short crack growth rate and is contributing to the enhanced fretting fatigue resistance. For this to be a possible reason, the crack growth resistance shown in the coarser microstructure would need to extend to the earliest crack (short crack) development and by a greater stress intensity threshold compared to a finer microstructure, crack initiation. Even though this author could not find specific crack initiation information for IN-100, the data shown from this test suggest a larger grain size has an enhanced resistance to short crack propagation and initiation.

Table 5.1 Results of fretting and plain fatigue

Test	Type	Pad	P	Stress Max	Q_{max}	Stress Min	Q_{min}	Stress Range	Effective Stress	Cycles to Failure
		mm	N	MPa	N	MPa	N	MPa	MPa	
1	Fretting Fatigue	50.8	4003	550.00	832	16.50	-365	533.50	542.51	7,000,000
2	Fretting Fatigue	50.8	4003	600.00	471.5	18.00	-93	582.00	591.83	2,511,439
3	Fretting Fatigue	50.8	4003	650.00	478.2	19.50	-711.7	630.50	641.15	750,028
4	Fretting Fatigue	50.8	4003	750.00	n/a	22.50	n/a	727.50	739.79	n/a
5	Fretting Fatigue	50.8	4003	800.00	598.3	24.00	-1100	776.00	789.11	207,938
6	Fretting Fatigue	50.8	4003	950.00	844.7	28.50	-1104	921.50	937.07	66,181
7	Fatigue			600.00		18.00		582.00	591.83	n/a
8	Fatigue			650.00		19.50		630.50	641.15	1,208,767
9	Fatigue			800.00		24.00		776.00	789.11	313,646
10	Fatigue			1050.00		31.50		1018.50	1035.71	53,210

Table 5.2 Comparison of cycles to failure between fretted and plain fatigue

Stress Range MPa	Fretting Fatigue Life	Plain Fatigue Life	% Difference
630.5	750,028	1,208,767	38.0
776	207,938	313,646	33.7
921.5	66,181		
1018.5		53,210	

Table 5.3 Half contact width comparison

	$a_{analytical}$	$a_{experimental}$	%
Test	mm	mm	Difference
2	0.60534	0.6	0.9
3	0.60942	0.605	0.7
4	0.60908	0.645	-5.9
5	0.6067	0.68	-12.1

Table 5.4 MSSR Results Fine Microstructure

Test	Test Type	Max Axial Stress (MPa)	MSSR	θ	x/a	N_f
1	Fretting	550	36.08	25	9.60E-01	7000000
2	Fretting	600	35.4	24	9.60E-01	2511439
3	Fretting	650	36.71	25	9.60E-01	750028
4	Fretting	800	40.32	25	9.60E-01	207938
5	Fretting	950	43.704	26	9.60E-01	66181
8	Plain	650	34.5			1,208,767
9	Plain	800	37			313,646
10	Plain	1050	40.2			53,210

Table 5.5 MSSR Results Coarse Microstructure

Test	Test Type	Max Axial Stress (MPa)	MSSR	θ	N_f
1	Fretting	650	38.16	138	5,900,000
2	Fretting	750	39.82	138.8	815,449
3	Fretting	800	40.5	137.9	245,000
4	Fretting	850	41.09	137.2	134,103
5	Fretting	950	42.66	139.7	77,937
10	Plain	885	37.5		509,166
11	Plain	944	39		216,993
12	Plain	1062	40.5		95,671
13	Plain	1080	41		91,950

Table 5.6 Effect of grain size on fatigue in nickel-based superalloys

Grain Size	ΔK_{th}	Crack growth	Grain size	Near threshold crack growth rate	Early (Non-Linear) Crack Propagation Rate	Linear Crack Growth Rate
Fine	lower	planar	6 micron	higher	much faster	faster
Coarse	higher	tortuous	55 micron	lower	much slower	slower

Table 5.7 Effect of grain size on titanium based alloy Ti6242

Grain Size	ΔK_{th}	Crack growth	Grain size	Near threshold crack growth rate	Early (Non-Linear) Crack Propagation Rate	Linear Crack Growth Rate
Fine	lower	planar	smaller	lower	much slower	faster
Coarse	higher	tortuous	larger	higher	much faster	slower

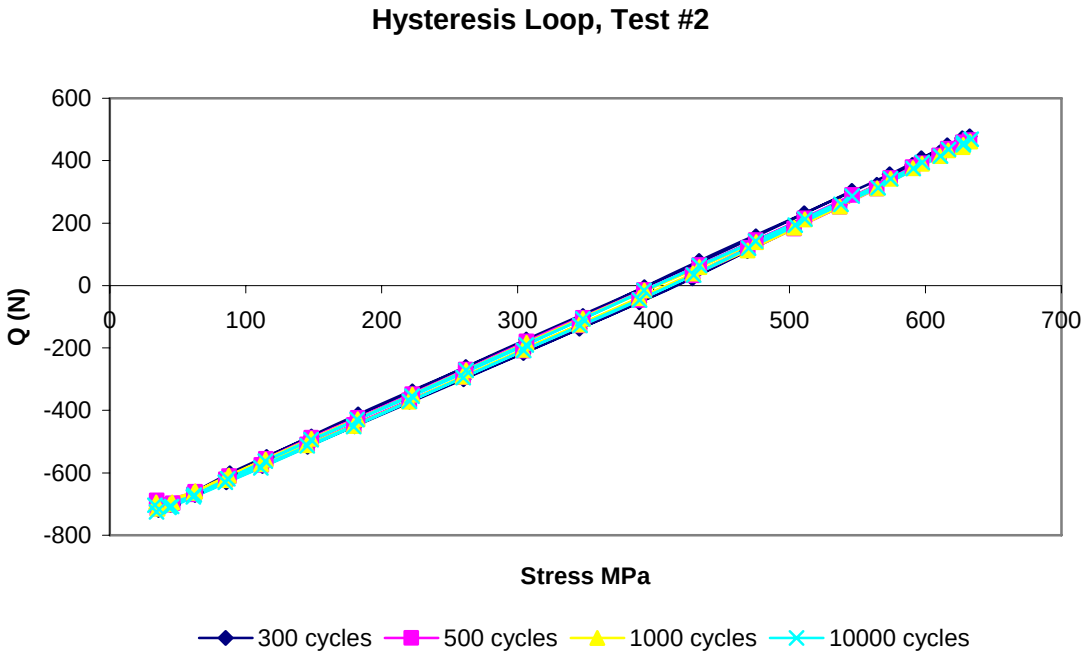

Figure 5.1 Hysteresis Loop of Test #2

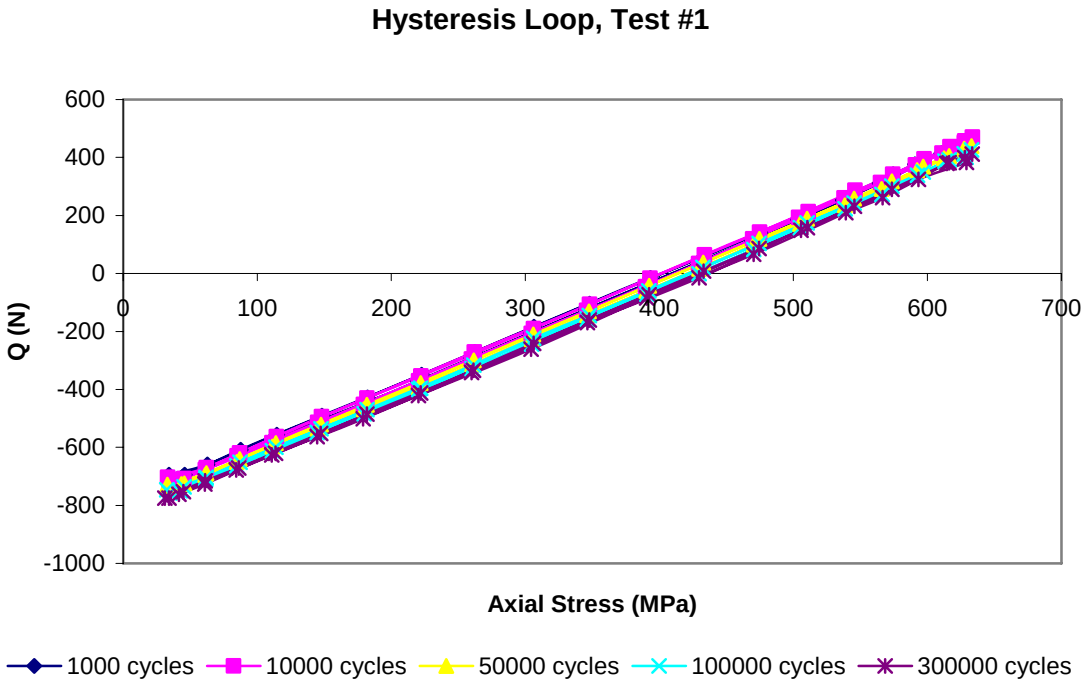

Figure 5.2 Hysteresis Loop of Test #1

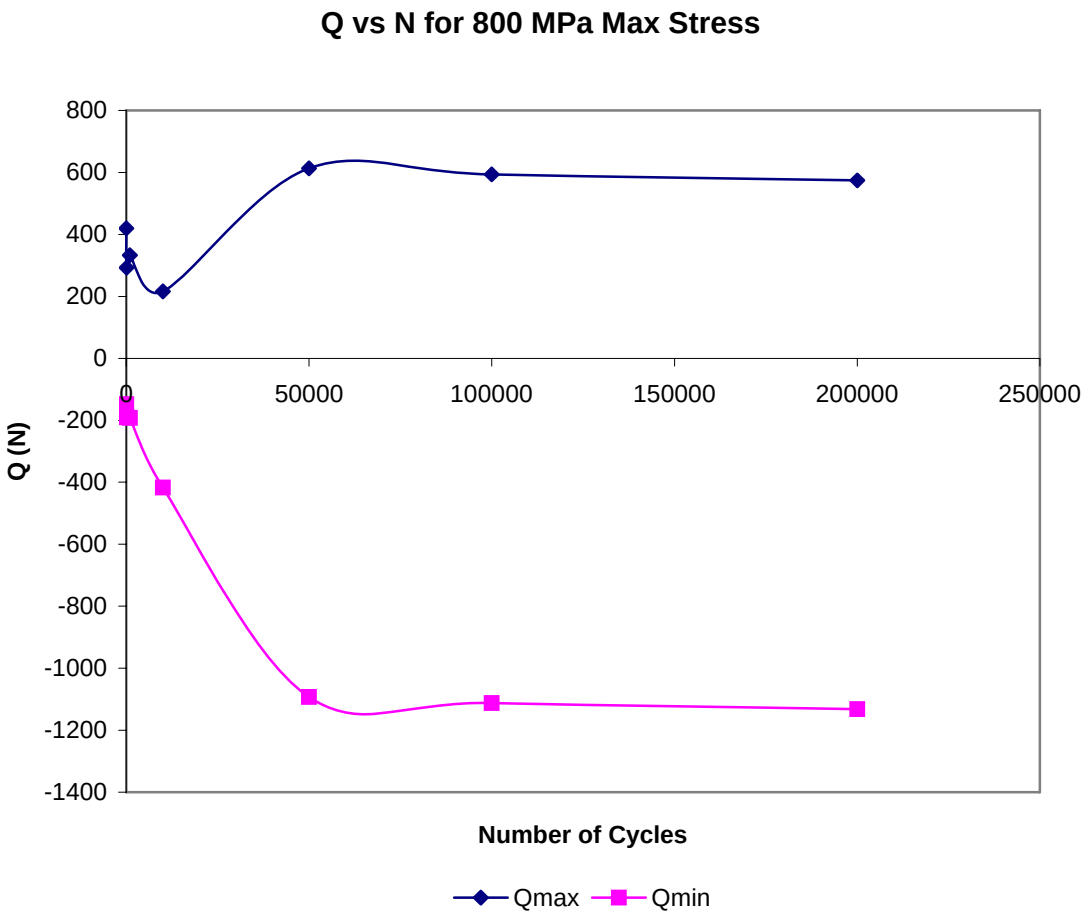

Figure 5.3 Q vs. N for Test #5

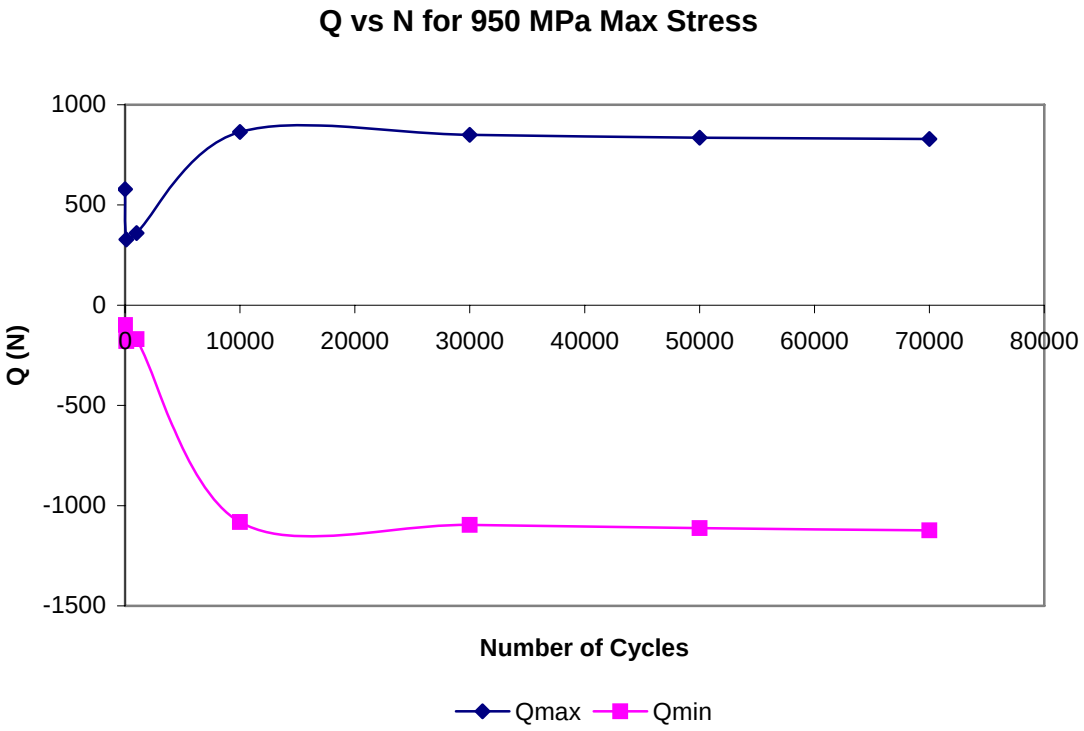

Figure 5.4 Q vs. N for Test #6

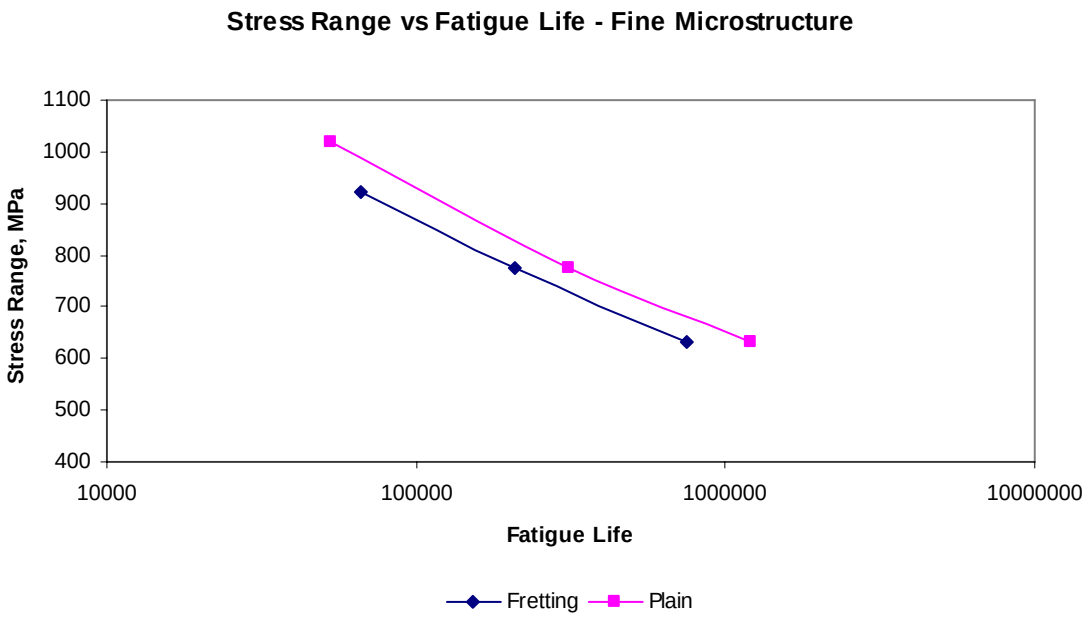

Figure 5.5 Fretting and plain fatigue S-N Curve – IN-100 This Study

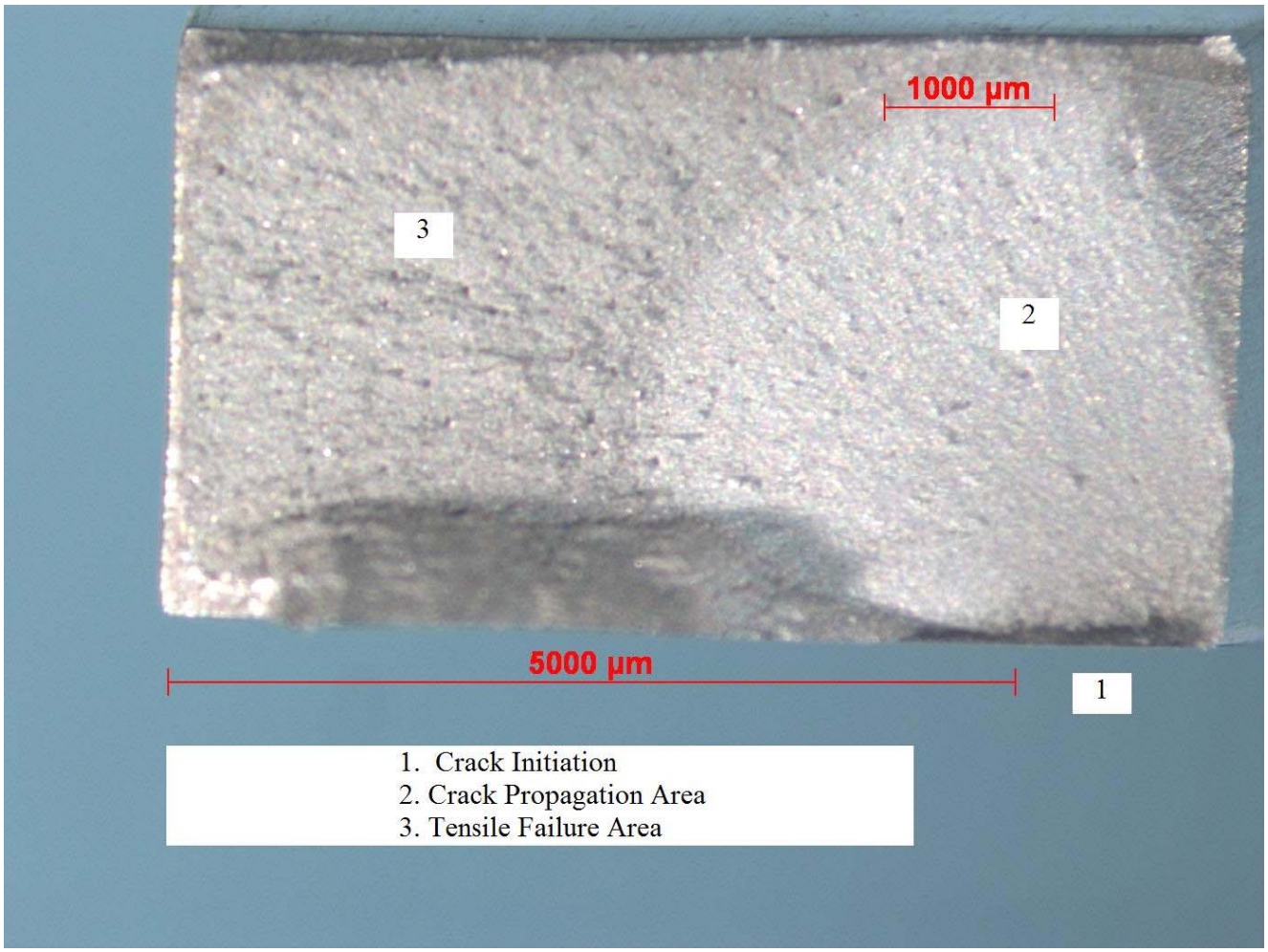

Figure 5.6 Three distinct areas are shown during fracture progression.

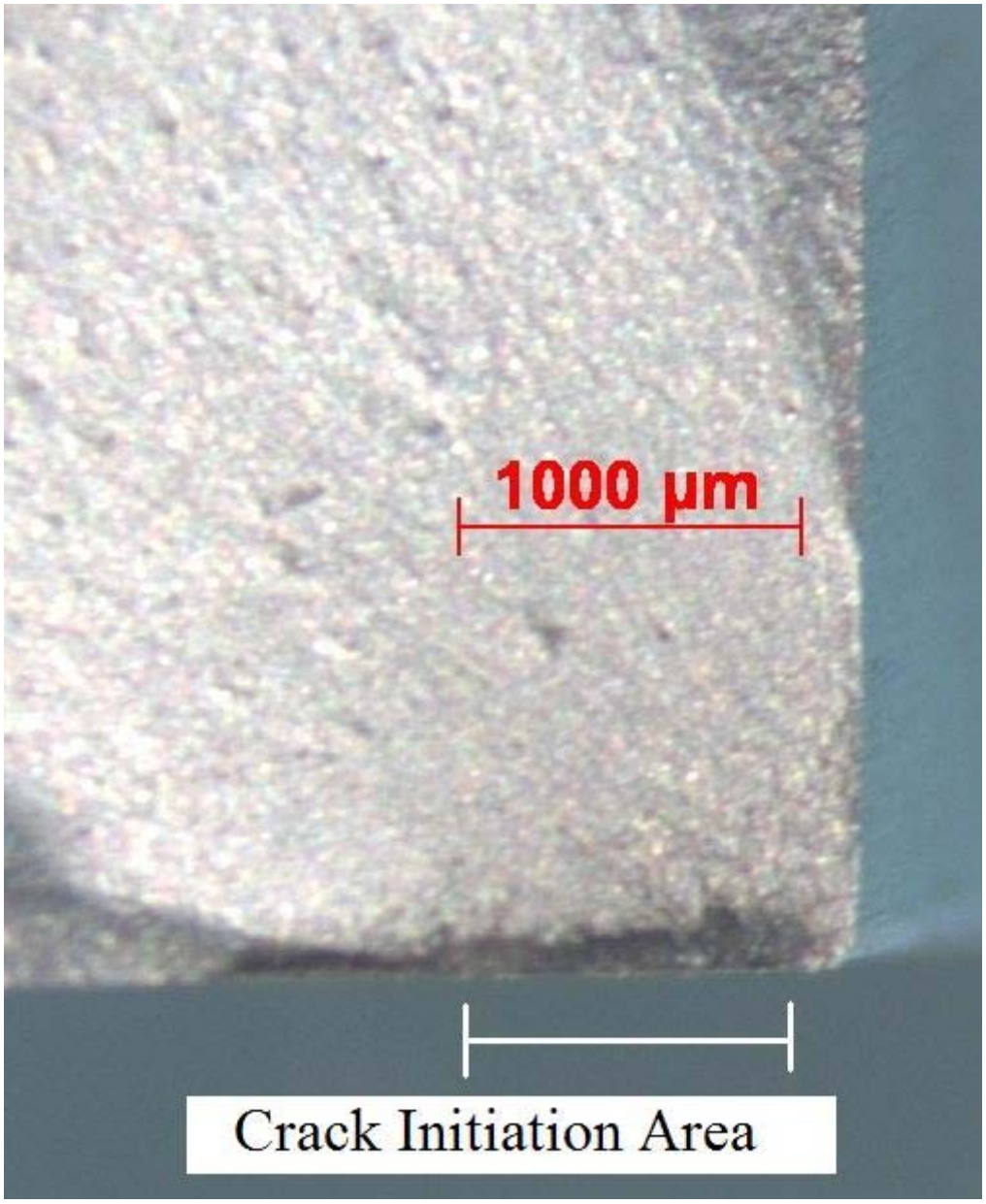

Figure 5.7 Crack initiation location

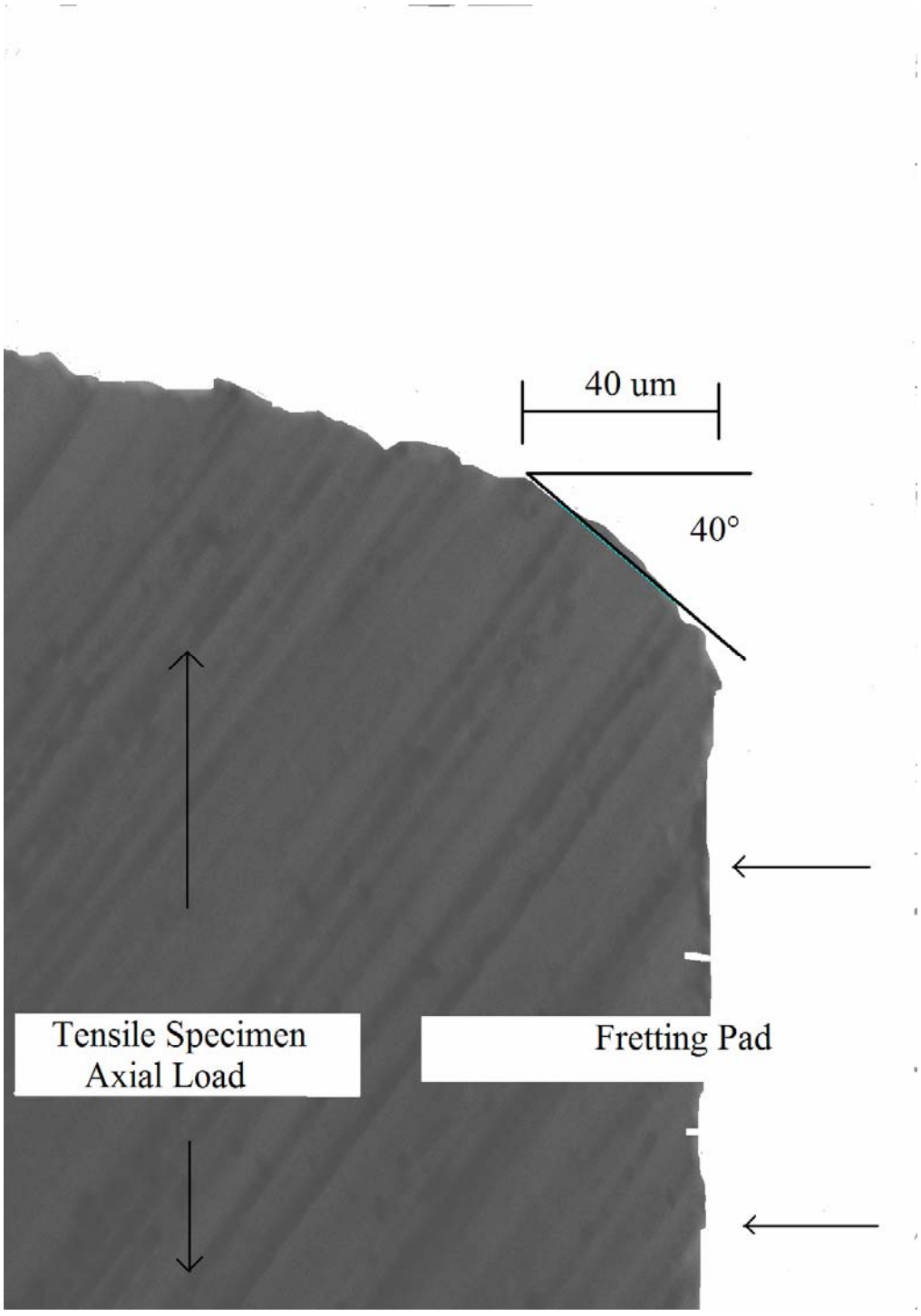

Figure 5.8 Crack initiation angle

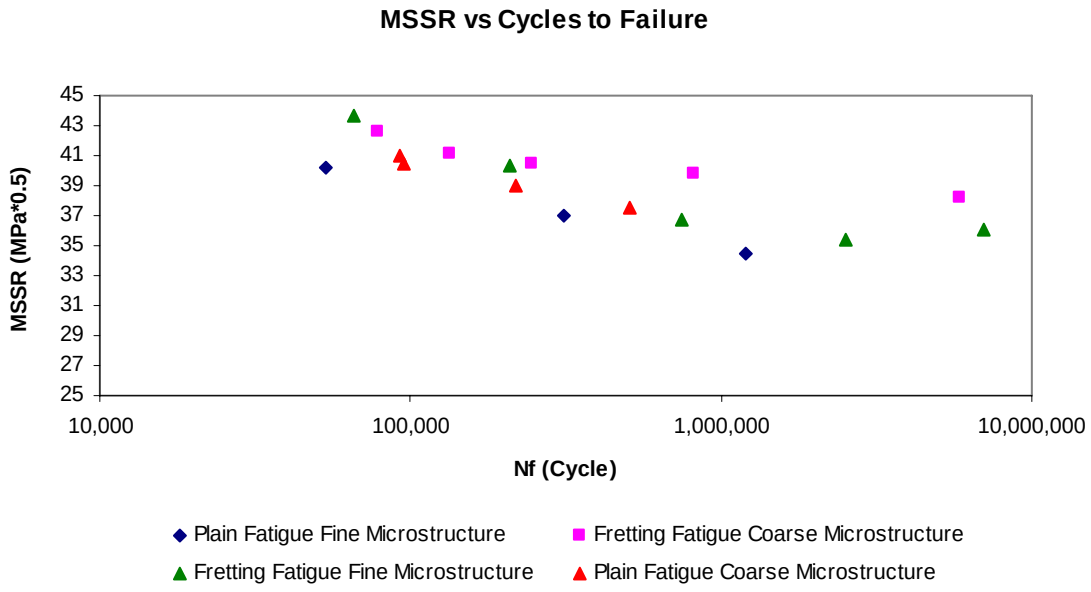

Figure 5.9 MSSR data for IN-100

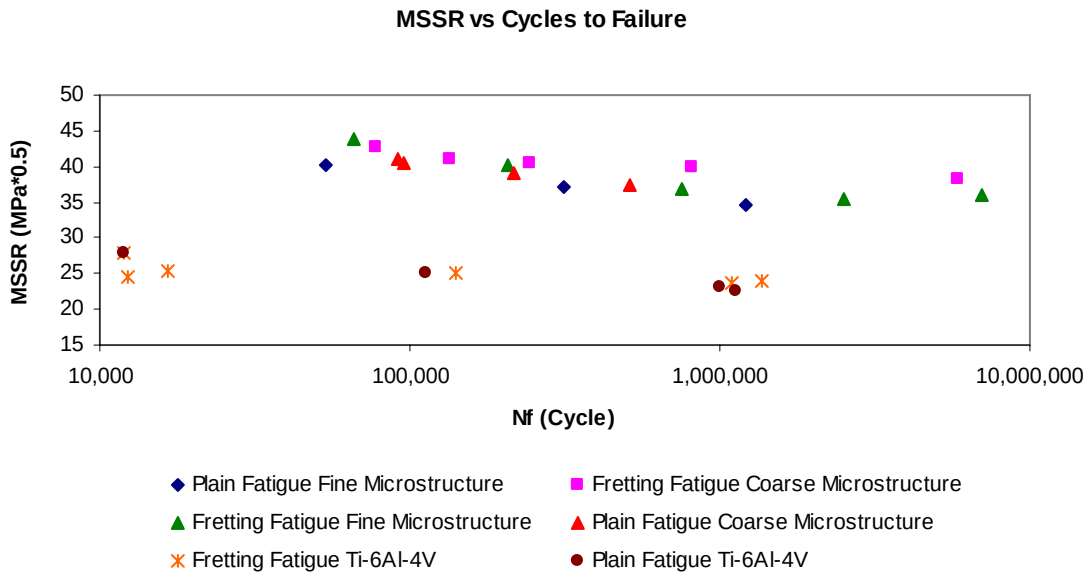

Figure 5.10 MSSR data for IN-100 and Ti-6Al-4V

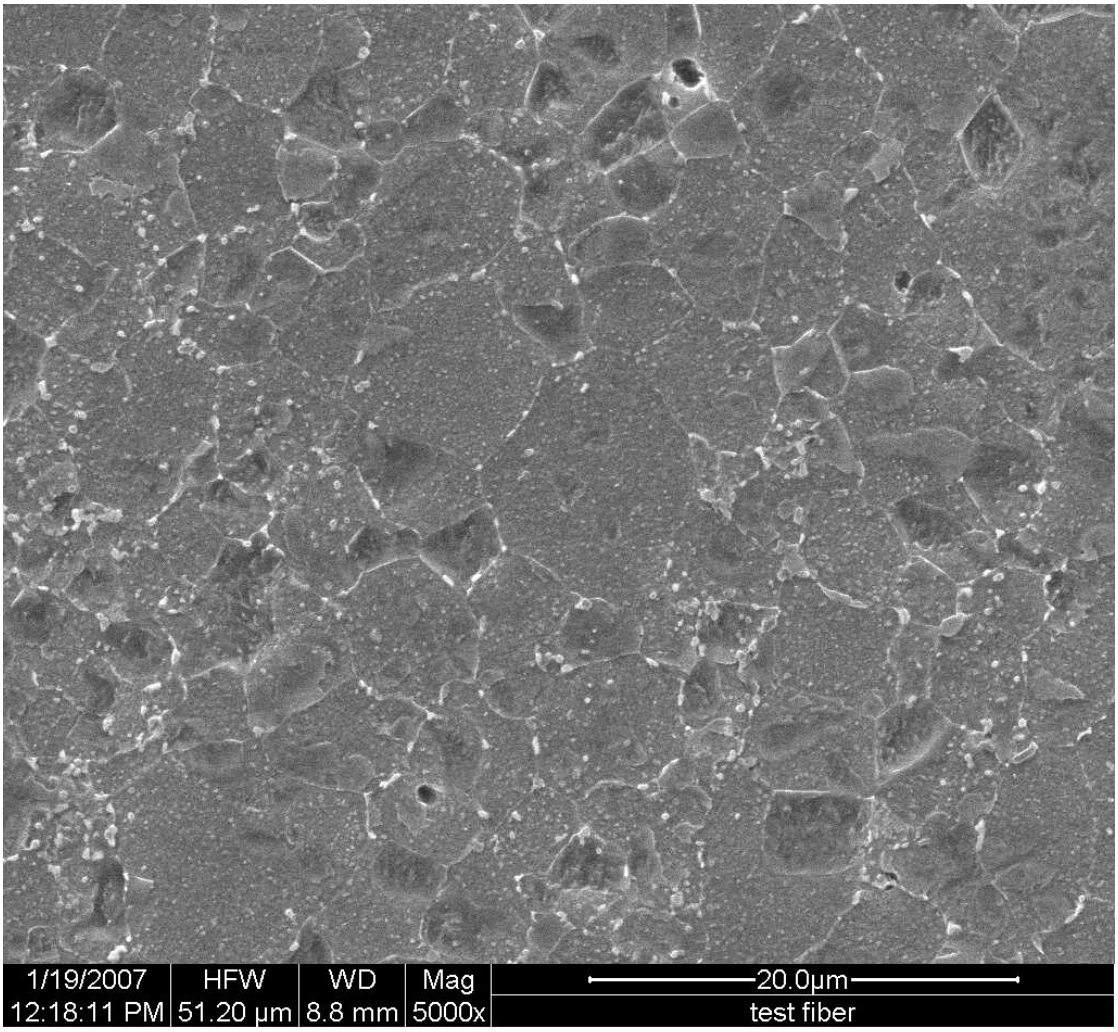

Figure 5.11 Seven micron average grain size microstructure

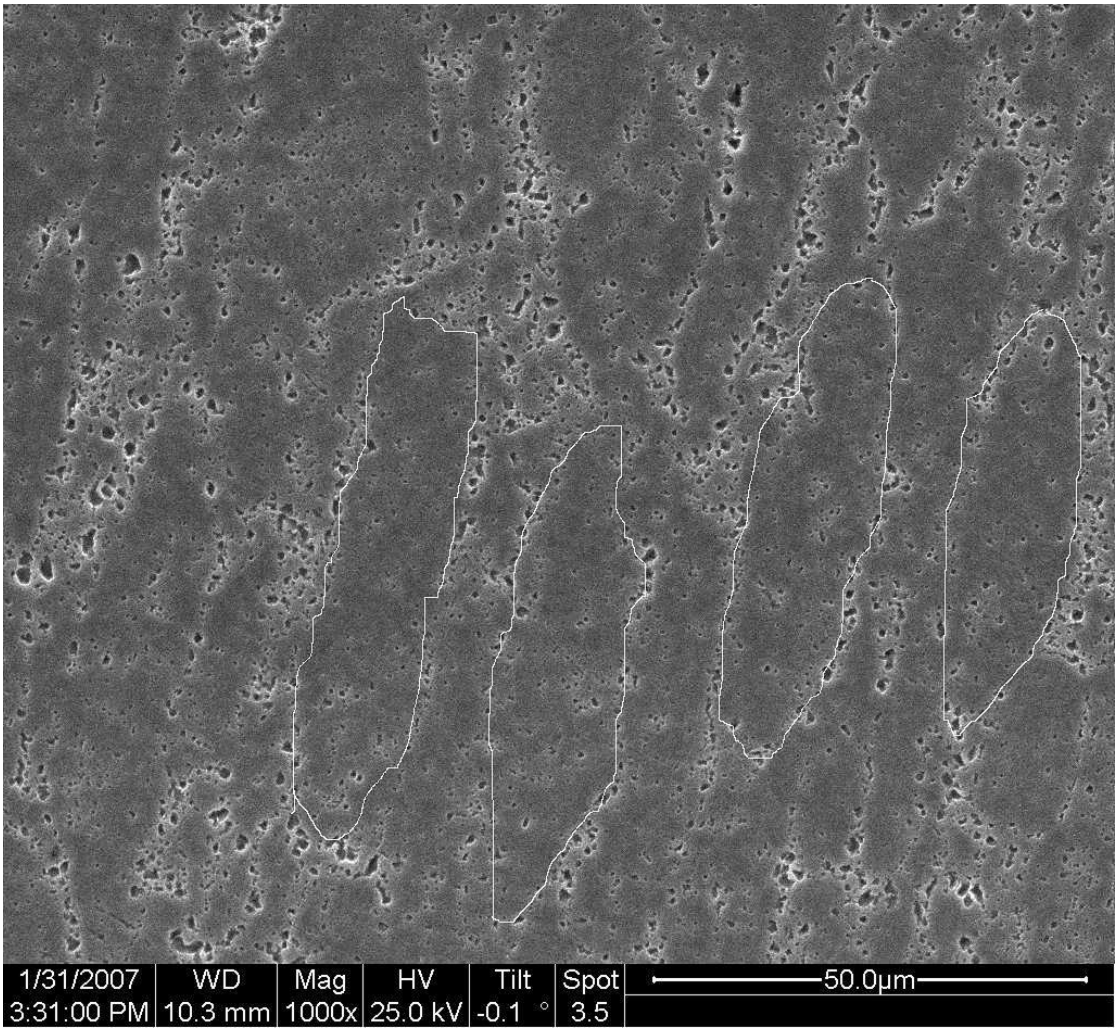

Figure 5.12 Fifty micron oblong grain material, four grains are enhanced to show boundaries.

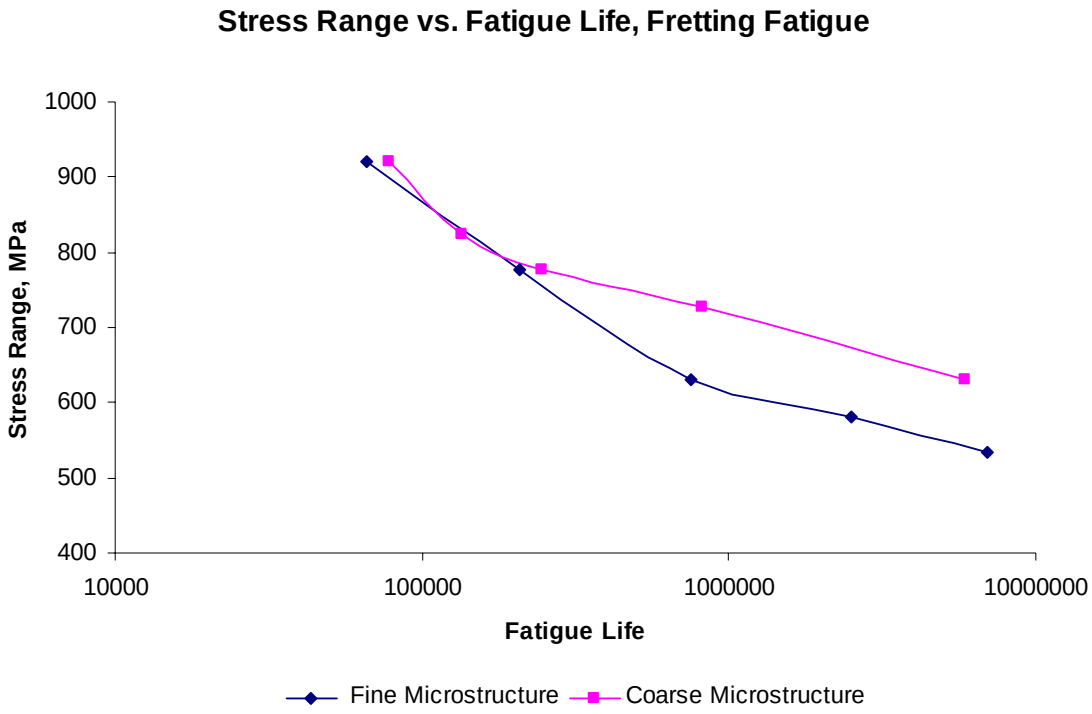

Figure 5.13 Fretting fatigue results of coarse and fine microstructure IN-100.

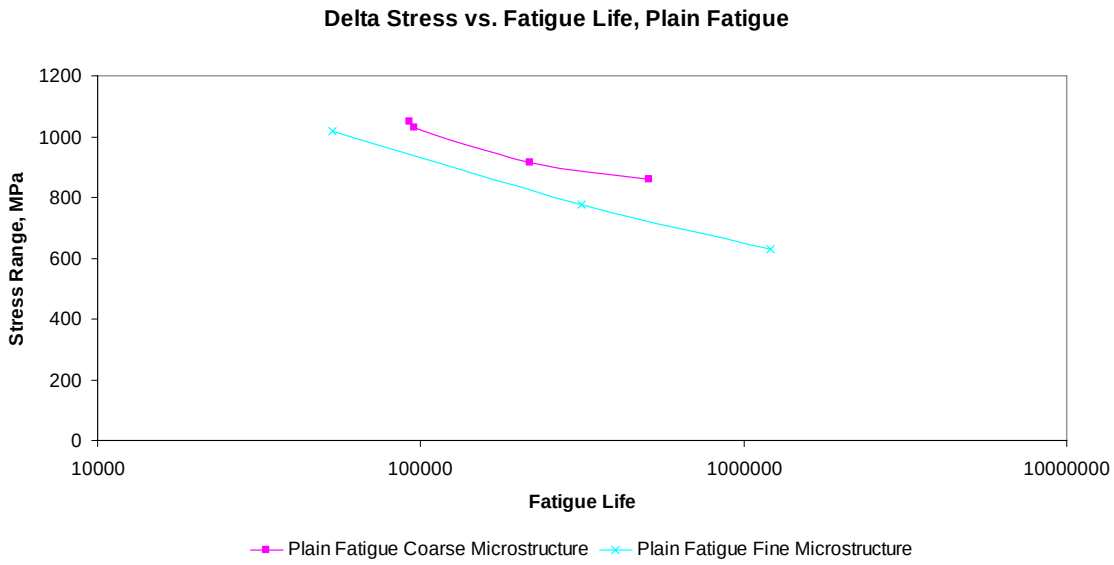

Figure 5.14 Plain Fatigue Comparison of IN-100 in coarse and fine microstructure

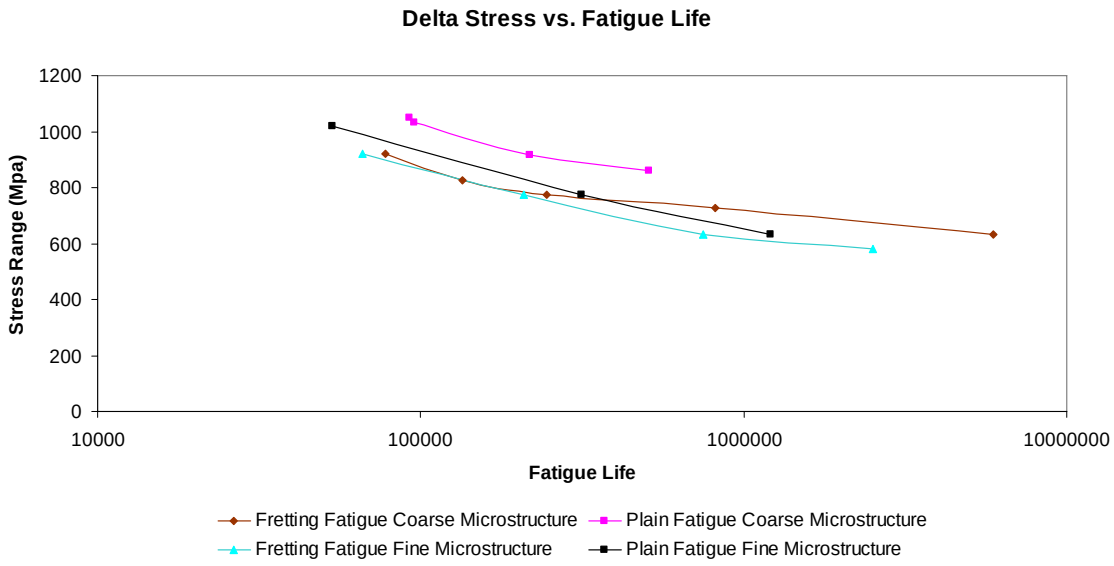

Figure 5.15 Fretting and Plain Fatigue data for Fine and Coarse Microstructure

VI. Conclusions and Recommendations

This chapter will summarize the conclusions of this study and follow with a set of recommendations for further work. First a summary of the tests will be given, followed by how the data was collected and analyzed. Second, a summary of the computational work done in this study will be outlined. Third, the microstructures of the two alloys studied will be summarized, then the conclusions from the study will be listed. Finally, recommendations for future work building on this study will be given.

6.1 Summary

The main objective of this test was to determine the change in fretting fatigue behavior of IN-100 with changes to microstructure. A total of 8 tests were conducted and used to define two S-N curves. The first, was a fretting fatigue curve at σ_{max} = 950 MPa to 550 MPa. A constant normal load of 4003 N was applied to the test specimens, and each test used the same R-ratio of 0.03. All fretting tests used a 50.8 mm cylindrical fretting pad and used the same servo-hydraulic controlled load frame to control the axial load. The plain fatigue tests were run on the same load frame as the fretting fatigue tests with the same R-ratio and a σ_{max} =1050 MPa to 650 MPa. The load frame was controlled by the software program Mutli-Purpose Test Software, which controlled the maximum and minimum loads applied to the specimen. The same sine wave form and 10Hz cycle speed was used for all tests. The software recorded cycles and maximum and minimum loading on each specimen until failure was reached. The experimental values obtained from the test software were used to find the tangential load on each specimen. The

tangential loads were used as inputs along with the normal load into the analytical and finite element programs used to find the stress state in the specimen and pad contact zone. The crack initiation angle and orientation were experimentally found and measured.

The analytical program Ruiz and a finite element program were used to find the stress states, σ_{xx}, σ_{yy} and τ_{xy} found locally across the contact region. The two solution methods were then compared against each other. The Ruiz program also found the contact half width and this was compared against experimental results. The Ruiz program was used to find the Shear Stress Range (SSR) and the Modified Shear Stress Range (MSSR). The results of the MSSR were compared to the experimental findings. The SSR was compared to the MSSR to compare the results of each parameter.

Next, two microstructures of IN-100 are compared to evaluate how the fretting fatigue behavior changes with microstructural changes. A finer grained material is compared to a coarser grained material. Conclusions were drawn for crack initiation, propagation and growth relative to the microstructure. Finally, the conclusions found for IN-100 fretting fatigue behavior were compared to titanium alloys tested in fretting fatigue and evaluated relative to microstructure.

6.2 Conclusions

1. In all cases, fretting reduced fatigue life compared to plain fatigue. For identical maximum and minimum stresses and R-ratio, the cycles to failure were reduced. In the

case of fatigue tests high cycle to fatigue region, the reduction in cycles to failure was about 35%. IN-100 shows degradation in fatigue life when fretting is introduced, as is common in other materials such as titanium alloys.

2. The crack initiation location for all tests was at the trailing edge, approximately at x/a = +1.

3. The crack initiation orientation was experimentally found to be 40°. This angle agrees with the crack initiation angle commonly found in titanium alloys of 45° +/- 15°.

4. The failure surface was found to have three distinct regions, crack intiation, propagation and finally, ultimate failure.

5. The Ruiz program was used to find the contact half width with less than 12.1% error compared to the experimental findings even though the specimens used disregarded the dimensional assumptions required for the program to give accurate results.

6. The Ruiz program gave σ_{xx}, σ_{yy} and τ_{xy} curves describing the contact region with less than 12% error compared to the more accurate finite element program.

7. The Modified Shear Stress Parameter was able to accurately predict the crack initiation location. The MSSR was not able to accurately predict the crack initiation angle, giving an angle 15° less than the experimentally found angle of 40°. Changes in

microstructure did not affect the MSSR parameter. The MSSR values for IN-100 are different than for titanium and MSSR values generated for titanium show some representation of IN-100 behavior but may work better in the constants used were modified for IN-100.

8. The fretting fatigue curve of a finer grained IN-100 was compared to a coarser grained IN-100 microstructure. The following was concluded:

a. Grain size had an effect on fretting fatigue characteristics, precipitate location, size or distribution did not have an effect on fretting fatigue.

b. The crack initiation behavior is dependent on microstructure.

c. The crack propagation behavior is dependent on microstructure. The coarser grained material had a slower non-linear crack propagation and linear crack propagation.

10. The fretting fatigue behavior of IN-100 is different than titanium based alloys in the following ways:

a. Titanium alloy microstructures have an effect on fretting fatigue based on grain size and alpha/beta lamellae size. IN-100 microstructures have an effect on

fretting fatigue based on grain size, other microstructural components such as precipitates do not have an effect.

b. Finer grained titanium alloy has better short crack growth resistance. Since fretting is largely dependent on crack initiation and short crack growth, fine grained titanium is favorable for fretting fatigue resistance. In IN-100 the affect of grain size appears to be opposite of titanium alloys. The behavior of the coarse grained IN-100 appears to be similar to the fine grained Ti-6Al-4V, with a slow short crack growth as a reason for the enhanced fretting fatigue resistance.

c. Finer grained titanium alloys and nickel-based superalloys have a more planar crack growth as grain size is reduced but in nickel-based superalloys, the effect of the planar growth is a faster non-linear crack propagation and linear propagation rate. In titanium alloys the effect of the planar growth is a slower non-linear early crack propagation rate with a linear crack propagation rate similar to a coarser grain sized titanium alloy.

d. In IN-100, microstructure is a significant factor in crack initiation and crack propagation, in titanium alloys, microstructure is significant in crack initiation but much less significant in crack propagation.

6.3 Recommendations for Future Work

1. The main purpose of this study was to develop a basic understanding of microstructural influences on the fretting fatigue behavior of IN-100. The current study focused on two specific microstructures at room temperature. The conclusions found for this study are at room temperature, however IN-100 is a high temperature metal and the effects of heat and microstructure can be evaluated with this study as a baseline of comparison.

2. The findings of this test suggest an attempt to better understand fretting fatigue crack initiation in IN-100 and other nickel-based superalloys should emphasize microstructure as a major influence on behavior. This study suggests the approach to understanding crack initiation should focus on microstructure as a significant factor.

3. This study has left some doubt in the ability of the modified shear stress range parameter to accurately predict the fretting fatigue failure of the fine grained IN-100 used in this study. The parameter worked well in every regard except the ability to predict the crack initiation angle and the placement of the fatigue curves relative to each other. Work in determining how well the parameter works for other microstructures of IN-100 would be beneficial. Also developing constants better representing IN-100 would benefit the development of the MSSR parameter for this material.

Appendix A. Modulus of Elasticity

The modulus of elasticity (E) for this material was found experimentally. A strain gage was adhered to a tensile specimen, then the specimen was elastically extended and relaxed before being extended again. The specimen was elastically extended to the following stresses: 300 MPa, 400 MPa, 500 MPa and 600 MPa, the recorded strains are recorded in Table A.1. Next, the applied stress was graphed against the measured strain and the resulting slope was recorded. Figure A.1 shows the resulting graph, showing a good linear relationship. The slope of this line, the value of E, is 201.93 GPa.

Table A.1 Recorded Strains at a given Stress and Resulting value of the Slope E

Stress (Pa)	Strain	Slope (Pa)
3.00E+08	1.47E-03	2.0193E+11
4.00E+08	1.97E-03	
5.00E+08	2.46E-03	
6.00E+08	2.96E-03	

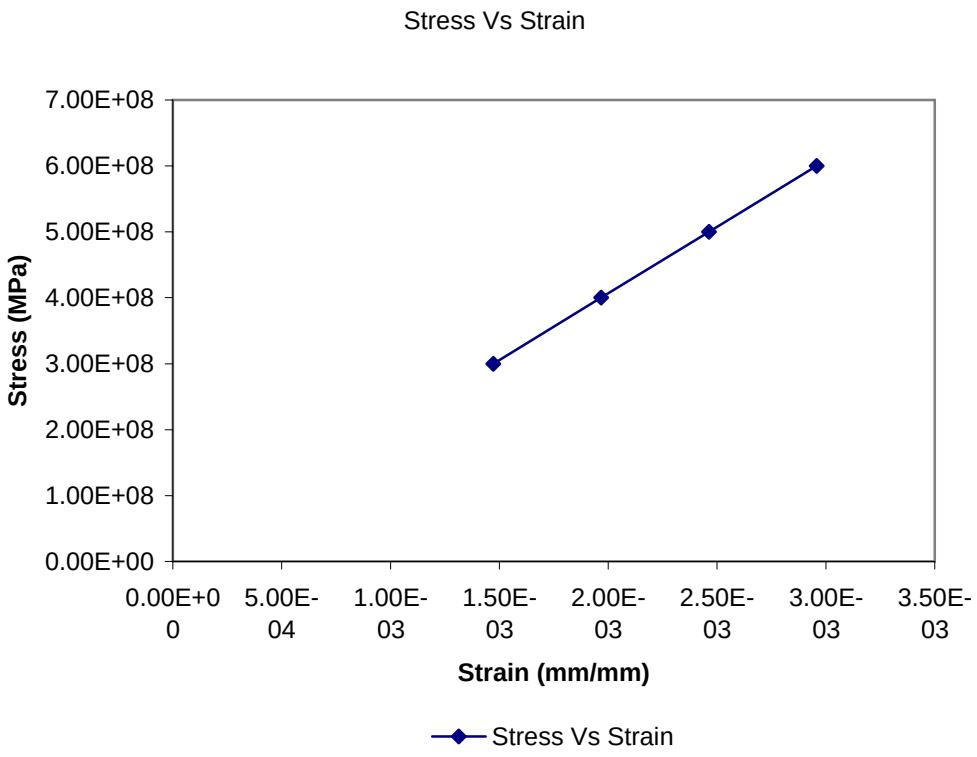

Figure A.1 Applied Stress versus Measured Strain

Appendix B – Fatigue Characteristics of KM4

In a study done by Padula et al, (21), the superalloy KM4 was used to evaluate fatigue characteristics for nickel-based superalloys. Figure B.1 shows the similarity this alloy has to IN-100 in composition. The findings from Padula's study found the finer grained material, in this case a sub-solvus heat treated material, designated as Sub (R=0.7) in Chart B.1, had a higher lower threshold da/dN and always had a higher crack propagation rate at a given ΔK compared to the super-solvus material, designated as Super (R=0.7). The crack propagation rates shown are for the same R-ratio, 0.7 and show the early (non-linear) fatigue propagation and linear Paris law crack propagation regions. In Figure B.2, the crack paths for KM4 are shown, notice in (a), the crack path for the finer 6 micron sized grain microstructure, the crack path is close to planar. In (b), the crack path for the coarser, 55 micron grained KM4 microstructure, the crack path is substantially more tortuous.

Table B.1 Composition of KM4 (21)

Element	wt%
Co	18
Cr	12
MO	4
Al	4
Ti	4
Nb	2
B	0.03
C	0.03
Zr	0.03
Ni	balance

Table B.2 Composition of IN-100

Element	wt%
Co	15
Cr	9.5
Mo	3
Al	5.5
Ti	4.75
V	0.95
Fe	0.2
Zr	0.06
W	0.04
Mn	0.01
Si	0.05
C	0.18
B	0.02
Ni	Balance

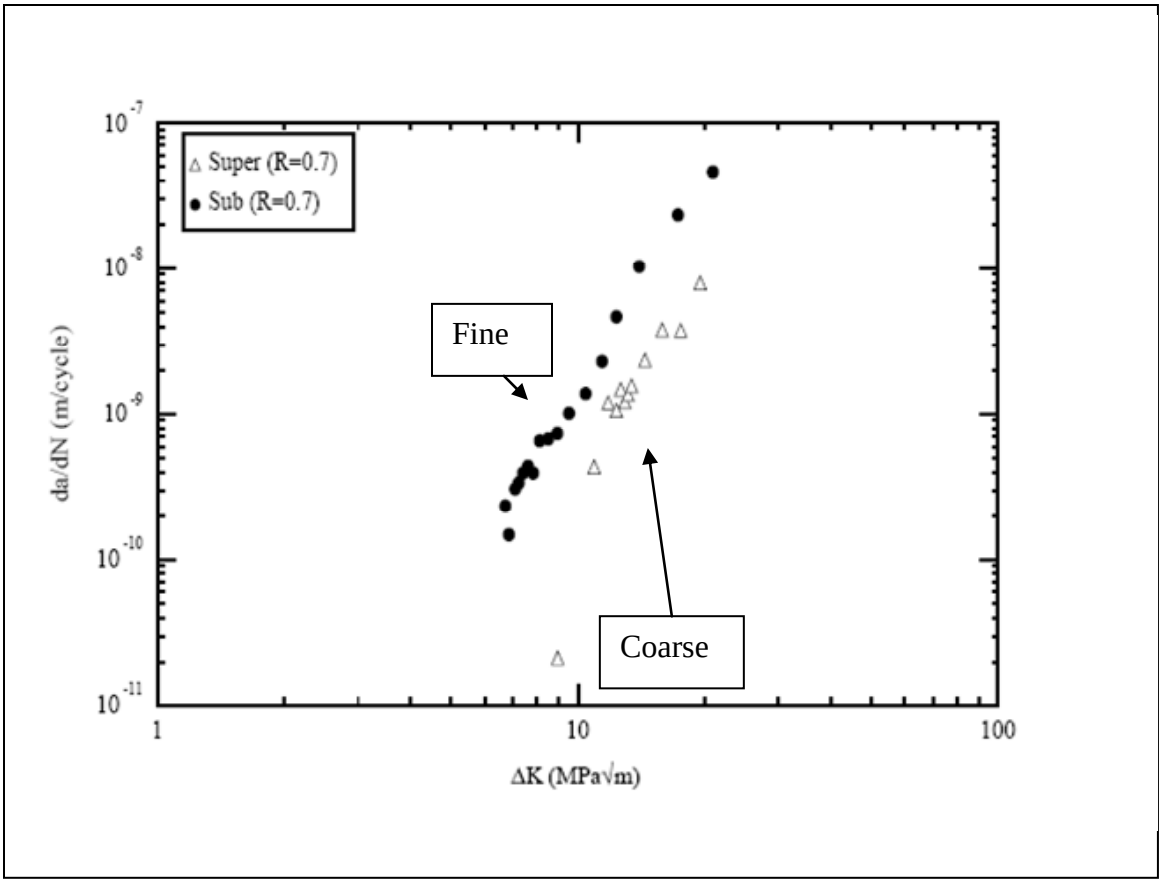

Figure B.1 The plot of da/dN versus ΔK for KM4 (21)

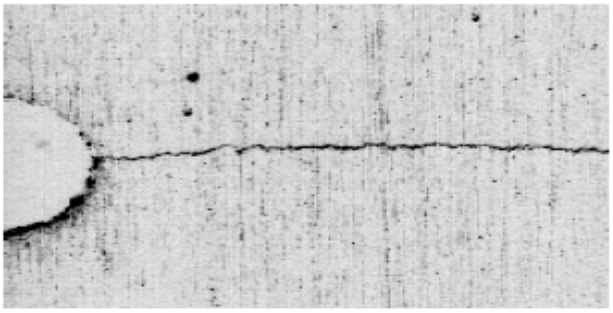

(a)

200 µm

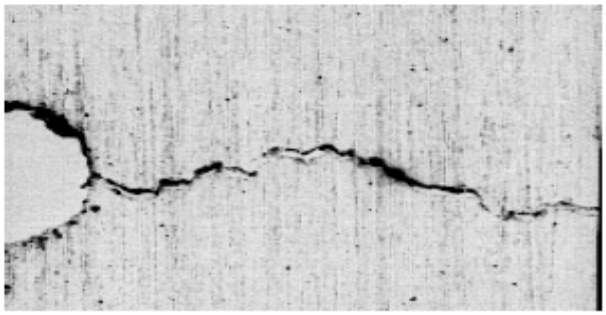

(b)

Figure B.2 Crack paths in KM4, (a) is for a finer grained material and (b) is for a coarser grained material. (21)

Appendix C-- Fatigue Behavior of Titanium Alloys

In a study done by Jin and Mall (23) on the titanium alloy Ti-6Al-2Sn-4Zr-2Mo-0.1Si (Ti6242), the fatigue characteristics are evaluated for the effect of microstructure on short crack growth behavior. The following Figure C.1 shows the effect of a fine and coarse lamellar microstructure on the crack propagation rate, da/dN and ΔK. The fine microstructure has a lower threshold da/dN compared to the coarse microstructure. It can also be seen that at a given ΔK, the fine microstructure will have a higher crack growth rate than the coarse structure and the finer structure has a lower ΔK threshold. Figure C.1 shows the non-linear early propagation and linear Paris law growth region. Figure C.2 shows the crack propagation paths for the fine (a) and coarse (b) microstructures. The scales are different and it can be seen that the fine microstructure gives a much less tortuous crack growth path.

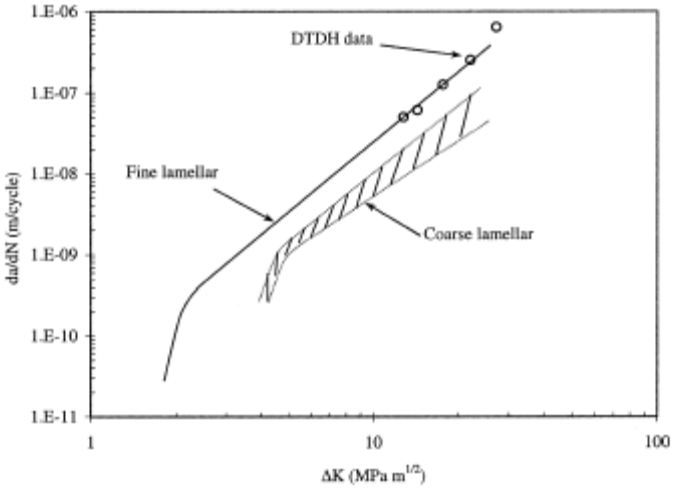

Figure C.1 The plot of da/dN versus ΔK for Ti6242 (23)

(a)

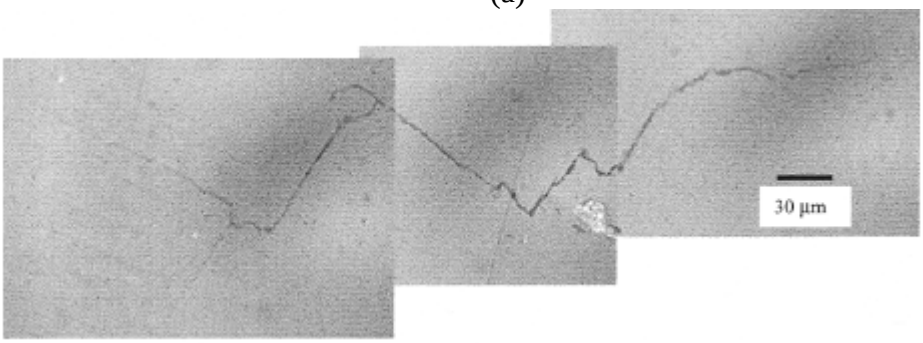

(b)

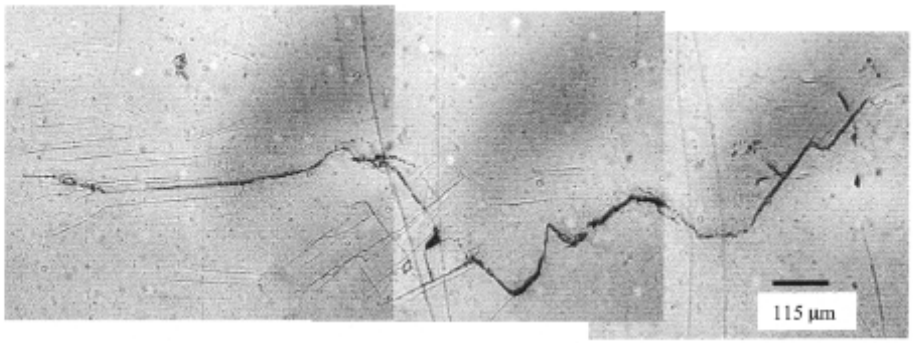

Figure C.2 Crack growth paths for a fine (a) and coarse (b) microstructure (23)

References

1. Koshal, D. Manufacturing Engineer's Reference Handbook. Butterworth-Heinemann Ltd, Oxford, England, 1993.

2. Donachie, M.J., Donachie, S.J.. Handbook of Materials and Selection. John Wiley and Sons, Inc., New York, 2002.

3. Hills, D.A., Nowell, D., and O'Connor, J.J. On the mechanics of fretting fatigue, Wear, (1988) 125, pp. 129-156.

4. Venkataraman, G., et al. Free energy formulation of fatigue crack initiation along persistent slip bands: calculation of S-N curves and crack depths. Acta Metall. Mater., 38, 1, 31-40

5. Mura, T., Nakasone, Y. *A* theory of fatigue crack initiation in solids. Journal of Applied Mechanics., (1990) 57, 1-6

6. Sakata, H. An application of fracture mechanics to fretting fatigue analysis. Proceedings of the International conference, 303-313. Amsterdam and New York, North Holland, 1987.

7. Hattori, T. Initiation and propagation behavior of fretting fatigue cracks. Proceedings of the 3rd International Conference on Contact Mechanics, 183-192. Madrid, Spain, July 1997.

8. Hills, D.A., Nowell, D. Mechanics of fretting fatigue, Kluwer Academic Publishers, Dordrecht, 1994.

9. Chan, K., Lee Y., Ruiz Program. South West Research Institute. Personal Communication, 1998

10. Namjoshi S.A., Mall, S., Jain, V., Jin, O. Fretting fatigue crack initiation mechanism in Ti-6Al-4V. Fatigue Fracture Engineering Material Structure. September 2001.

11. Madhi, E. Fretting fatigue behavior of nickel alloy IN-100. Master's Thesis, Wright Patterson Air Force Base, OH, March 2006.

12. Iyer, K., Mall, S. Effects of cyclic frequence and contact pressure on fretting fatigue under two-level block loading. Fatigue and Fracture of Engineering Materials and Structures. 23(ISSN 8756-758X):335-345, 2000.

13. Walker, K. The effect of stress relation during crack propagation and fatigue for 2024-Y3 and 7075-T6 aluminum. Presented to subcommittee E-9V Winter Meeting. 1969

14. Lykins, C.D. An investigation of fretting fatigue crack initiation behavior of the titanium alloy Ti-6Al-4V. Ph.D. dissertation, University of Dayton, OH, December 2004.

15. Sabelkin V., Mall, S., Sathish, S, Martinez, S., Blodgett, M. Effect of shot-peening intensity on fretting fatigue crack-initiation behavior of Ti-6Al-4V. Fatigue Fract Engng Mater Struct. September 2004.

16. Milligan, W.W., et al. Effects of Microstructure on the High Temperature Constitutive Behavior of IN 100., Superalloys 2004, pp. 331-339, The Minerals, Metals and Materials Society

17. Padula, S.A., Shyam, R.O., Ritchie, R.O., Milligan, W.W., High Frequency Fatigue Crack Propagation Behavior of a Nickel-Base Turbine Disk Alloy. International Journal of Fatigue, Dec. 1998

18. Huther, W., Reppich, B., Interaction of Dislocations with Coherent, Stress-Free Ordered Particles, Z. Metallkd., 19 (1978), 628-634

19. Jin, O., Mall, S., Effects of microstructure on short crack growth behavior of Ti-6Al-2Sn-4Zr-2Mo-0.1Si alloy, Materials Science and Engineering A359 (2003) 356-367

20. Weertman, J., Mechanics of Fatigue, T. Mura, ed., ASME, NY, 1981, pp. 11-19

21. Lin, G.M., Fine, M.E., Scripta Metall., 16, 1982, pp. 1249-1254

22. Sadananda, K., Shahinian, P., Int. J. Fracture, 13, 1977, pp. 585-594

23. Wan, J.S., Yue, Z.F. A low-cycle fatigue life model of nickel-based single crystal superalloys under multiaxial stress state. Materials Science and Engineering, A392:145-149, 2005

24. Shyam, A., Milligan, W.W. A model for slip irreversibility and its effects on the fatigue crack propagation threshold in a nickel-base superalloy. Acta Materialia, 53:835-844, 2005

25. Brien, V., Decamps, B. Low-cycle fatigue of nickel-based superalloy at high temperature: deformation microstructures. Materials Science and Engineering, A316:18-31, 2001

26. Piard, A., Gamby, D., Carbou, C. Mendex, J. A numerical simulation of creep-fatigue crack growth in a nickel-base superalloy. Engineering Fracture Mechanics, 71:2299-2317, 2004

27. Sondhi, S.K. et al. Tension-compression creep asymmetry in a turbine disc superalloy: Roles if internal stress and thermal aging. Acta Materiala, 52:1761-1772, Dec. 2004

28. Murphy et al. Fretting fatigue of single crystal/polycrystalline nickel subjected to blade/disk contact loading. Acta Astronautica, 57:1-9, 2005.

29. Hills, D., Nowell, D. Contact stress in a moderately thin strip (with particular reference to fretting experiments). Wear 185 235:238. 1995

30. Magaziner, R.S. Examination of contact width on fretting fatigue. Ph.D. dissertation, Graduate School of Engineering, Air Force Institute of Technology, Wright-Patterson AFB, OH, March 2002. AFIT/GAE/ENY/02-8

31. Mall, S., Namjoshi, S.A., Porter, W.J. Effects of microstructure on fretting fatigue crack initiation behavior of Ti-6Al-4V. Materials Science and Engineering (2004)

REPORT DOCUMENTATION PAGE			Form Approved OMB No. 074-0188
The public reporting burden for this collection of information is estimated to average 1 hour per response, including the time for reviewing instructions, searching existing data sources, gathering and maintaining the data needed, and completing and reviewing the collection of information. Send comments regarding this burden estimate or any other aspect of the collection of information, including suggestions for reducing this burden to Department of Defense, Washington Headquarters Services, Directorate for Information Operations and Reports (0704-0188), 1215 Jefferson Davis Highway, Suite 1204, Arlington, VA 22202-4302. Respondents should be aware that notwithstanding any other provision of law, no person shall be subject to an penalty for failing to comply with a collection of information if it does not display a currently valid OMB control number. **PLEASE DO NOT RETURN YOUR FORM TO THE ABOVE ADDRESS.**			
1. REPORT DATE *(DD-MM-YYYY)* 22 Mar 07	**2. REPORT TYPE** **Master's Thesis**		**3. DATES COVERED** *(From – To)* 23-Aug-05 – 22 Mar 07
4. TITLE AND SUBTITLE The Effect of Microstructure on Fretting Fatigue Behavior of Nickel Alloy IN-100			**5a. CONTRACT NUMBER** **5b. GRANT NUMBER** **5c. PROGRAM ELEMENT NUMBER**
6. AUTHOR(S) Saladin, Erik, C., Captain, USAF			**5d. PROJECT NUMBER** **5e. TASK NUMBER** **5f. WORK UNIT NUMBER**
7. PERFORMING ORGANIZATION NAMES(S) AND ADDRESS(S) Air Force Institute of Technology Graduate School of Engineering and Management (AFIT/EN) 2950 Hobson Way WPAFB OH 45433-7765			**8. PERFORMING ORGANIZATION REPORT NUMBER** AFIT/GMS/ENY/07-M02
9. SPONSORING/MONITORING AGENCY NAME(S) AND ADDRESS(ES) AFOSR/NA Brett Connor 875 N Randolph St Suite 325, Rm 3112 Arlington, VA 22203-1768 Conner, Brett Capt AFRL/AFOSR [brett.conner@afosr.af.mil]			**10. SPONSOR/MONITOR'S ACRONYM(S)** **11. SPONSOR/MONITOR'S REPORT NUMBER(S)**
12. DISTRIBUTION/AVAILABILITY STATEMENT APPROVED FOR PUBLIC RELEASE; DISTRIBUTION UNLIMITED.			
13. SUPPLEMENTARY NOTES			

14. ABSTRACT

This thesis studied the effect of microstructure on the fretting fatigue behavior of IN-100. First, fretting and plain fatigue S-N curves were determined over a large range of applied stress at an identical R-ratio and for fretting tests, done with a constant contact load. It was found that fretting fatigue reduces the cycles to failure compared to plain fatigue. The half contact width was found for the specimens, the crack initiation angle was found to be 40° and the crack initiation location was at the trailing edge of contact for the fretting specimens. Computational work included finding the stress profile in the contact region using an analytical method and a finite element method. The analytical method computed half contact width and was found to be in good agreement with experimental half contact width. The stress profiles produced from each method were compared and found to be in good agreement. The stress profiles were used to find the Modified Shear Stress Range (MSSR) Parameter. The MSSR parameter produced results in good agreement with the experimental data for crack initiation location and fatigue life. This study found microstructure did not have an effect on the MSSR parameter for IN-100. This study also found MSSR data developed for titanium alloys did not adequately represent IN-100. The parameter also gave reasonable agreement with the experimental finding for crack initiation angle. A microstructural evaluation was done between the 7 micron grain sized material of this study and an oblong, 10 by 50 micron grained microstructure IN-100 from a previous study. The study found microstructure did have an effect on crack initiation and crack propagation, with the coarser grain structure performing better in fretting fatigue. The coarser grain structure allowed a longer initiation and crack propagation time, possible reasons why include impeding crack development by a more tortuous crack path. These findings were different than in titanium alloys, where a finer grain structure allowed a longer crack initiation time by impeding crack development with a more tortuous crack path.

15. SUBJECT TERMS

Fretting Fatigue, Nickel-Based Superalloys, IN-100, Microstructure,

16. SECURITY CLASSIFICATION OF:			17. LIMITATION OF ABSTRACT	18. NUMBER OF PAGES	19a. NAME OF RESPONSIBLE PERSON
REPORT U	ABSTRACT U	c. THIS PAGE U	UU	130	Shankar Mall **19b. TELEPHONE NUMBER** *(Include area code)* (937) 255-3636, ext 4587; e-mail: shankar.mall@afit.edu